Theses and Dissertations

2013

Structural Analysis of an Archimedes Screw and a Kinetic Hydro Turbine

Zachary Kraybill
Lehigh University

Recommended Citation

STRUCTURAL ANALYSIS
OF AN ARCHIMEDES SCREW
AND A KINETIC HYDRO TURBINE

by

Zachary A. Kraybill

A Thesis

Presented to the Graduate and Research Committee

of Lehigh University

in Candidacy for the Degree of

Master of Science

in

Mechanical Engineering

Lehigh University

May 2013

This thesis is accepted and approved in partial fulfillment of the requirements for the Master of Science in Mechanical Engineering.

_____

Date Appoved

_____

Dr. Alparslan Oztekin

Advisor

_____

Dr. D. Gary Harlow

Department Chair Person

ACKNOWLEDGMENTS

TABLE OF CONTENTS

Table of Figures

ABSTRACT

Finite Element Analysis (FEA) can be a great tool for analyzing the structural integrity of any mechanical design. Paired with Computational Fluid Dynamics (CFD) the forces can be evaluated on a hydro turbine allowing for such an analysis. In this case, two micro hydro turbines were analyzed, an Archimedes Screw design, in the case of an available head, and a hydrokinetic design, aiming at extracting the kinetic energy of a river. The Archimedes Screw design features two non-uniform pitch blades with three rotations, a 19.5" runner length, and a 6" blade diameter, while the shape of the hydrokinetic design follows a more conventional design similar to a propeller using two blades with a NACA 8406 profile swept over 140 degrees with an average span angle of 70 degrees. Rotating frame of reference was a concept used in both simulation types to ease the computational modeling. For the Archimedes Screw design this test was conducted at a volumetric flow rate of 0.1 m^3/s and 1000 RPM, while for the hydrokinetic design this test was conducted at a flow rate of 4.0 m/s and 225 RPM. Pressure distributions were imported from CFD simulations, fixed supports were used at the edge of the shaft, and tetrahedral elements were used. In the case of both designs, changes were made in order to improve the structural integrity based on the findings of the FEA study. Factors of safety of each design ultimately were at the least 1.5, given that the studies were completed under the highest loading rather than the optimal loading. Further the deflection found at the tip of the blade in hydrokinetic design reached 8 mm, which is enough to be concerned about the accuracy of the power and efficiency as well as the dynamic stability.

Chapter1: Introduction
History of Hydropower

Hydropower has a lengthy history and is an integral type of energy production especially with the need for sustainable, green energy sources. Dating back over two millennia, Greeks first began using water wheels to grind wheat into flower [1]. Unchanged for thousands of years, hydropower again resurfaced as a source of energy in the form of hydroelectric plants, the first being Niagara Falls followed by the Theodore Roosevelt Dam [1]. Between the early 1900's and the 1940's, hydropower was on the rise, eventually accounting for approximately 40% of the United States' energy sources. With more hydroelectric plants being created regulation began to take place after World War I with developments in thermal plants, transmission, and distribution [1]. In the 1930's more dams were built including the Grand Coulee Dam and the Hoover Dam [1]. Despite a steady reduction in usage, today hydropower still accounts for 10% of the energy sources of the United States [1].

Due to a diminishing availability of fossil fuels as well as associated direct environmental concerns such as the burning of gasoline and the indirect environmental concerns such as oil spills and rupture of natural gas pipelines, the desire for new sustainable and environmentally friendly sources of energy has grown substantially. There are several disadvantages to hydropower and these are primarily environmental. Dams block migratory routes for some fish, and the creation of dams cause significant changes to the landscape, primarily the rivers themselves and forests surrounding these rivers [2]. The destruction of these forests lead to the production of harmful gases in

addition to the habitat of species living in these forests [2]. Dams reduce nutrient flow downstream as well as the oxygen levels which can cause significant disturbance to plant and animal life, both aquatic and land [2]. Most of the drawbacks associated with hydropower, while not all, apply primarily to the dams created in order to create the pressure differential which is the driving force in the large turbines conventionally used. This has led to a distrust of hydropower in the public mind.

Amongst all these disadvantages, there are a number of serious advantages to hydropower. Hydropower is a fully renewable resource. Relying solely on the natural cycle of water in the form of evaporation and precipitation, there is no conceivable end to the energy that can be generated by hydropower [2]. Hydropower facilities also produce no air pollution, and specifically no carbon dioxide emissions [2]. Despite high costs associated with the development and implementation of hydropower plants, these plants, over a lifetime, generally have a lower associated cost than nuclear power or fossil fuels due to the low operating costs [2].

Types of Turbines

There are a number of hydropower turbines generally in use. These fall into two major categories, impulse turbines and reaction turbines. Reaction turbines rely on a pressure differential, whereas impulse turbines are not fully immersed in water and a high pressure, stream of water hits each blade individually bucket of the blade [3]. Two types of impulse turbines are Pelton and cross-flow. Pelton turbines, seen in Figure 1, have at least one jet of high pressure water stream directly onto the blade [3]. Cross-flow

turbines allow water to flow through the blade twice, once when the water flows from the outside of the blade inwards, and a second time from the inside outwards. The cross-flow turbines allow for lower higher flow rates and lower heads than the Pelton alternative [3].

Figure 1: Pelton Turbine [4]

Compared to impulse turbines, reaction turbines generally allow for higher flow rates and lower pressure differentials. Types of these turbines include Kaplan, Francis, and kinetic turbines [3][5]. As seen in Figure 2, the Kaplan turbine features a design similar to conventional propeller blades used in boats. Water is directed through the wicket gates tangentially and then is directed in the axial direction, downwards through the turbine blades causing them to rotate [5]. Where the Kaplan turbines feature somewhere in the range of three to six blades, the Francis turbine usually has upwards of nine blades, generally referred to as buckets [5]. Both types cause a significant reduction in the pressure. This requires a significant amount of head built up, often by dams.
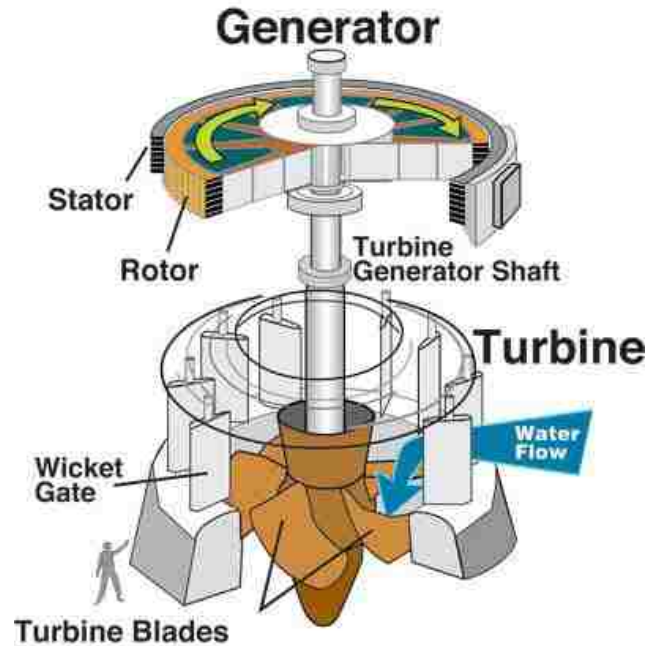
Figure 2: Kaplan Turbine [5]

Kinetic is the third main type of reaction turbines. Contrary to other reaction turbines, this type of turbine does not require a pressure gradient through the system. Rather these turbines use only the kinetic energy of the water flow to turn the blades [5]. Although less efficient, these have a variety of application such as rivers, tidal and ocean waves, and man-made channels due to the simplification of the process [5]. An added benefit is the lack of requirement of a man made structure such as a dam, removing many of the disadvantages to hydropower. It should be said that the downstream effect of oxygen levels as well as danger to aquatic life are still present disadvantages even with this system.

Micro Hydro Trends

The newest developments have tended towards small hydropower, sometimes referred to as micro-hydro. This can either refer to a small instillation placed next to a river taking advantage of the natural elevation change of the river, as seen in Figure 3, or a simple kinetic turbine placed in the river. Small hydro instillations are advantageous as they have minimal impact on the landscape and they have a much lower instillation cost, two of the biggest deterrents from the large hydro instillations [6]. In particular the relatively low cost and effect on agriculture are two main reasons why these small hydro instillations are particularly desirable in less developed countries [6]. Additionally Europe and China have a considerable number of sites available for small hydro instillation, while very few remain for large hydro instillation [6]. China in particular has a great potential for small hydro. Due to the high amount of rural, mountainous regions in China, there are a lot of potential sites for small hydro instillations and despite already accounting for 40% of the world's small hydro instillations, the government has plans to continue to increase the number of these sites [6]. Kinetic turbines seem to serve a different need due to their small size, portability, and generally low cost. The portability allows for usage in disaster scenarios where a government agency would desire an easily installed energy source to power emergency equipment in the event that damage to the area's supply of electricity is compromised. The small size and low cost, on the other hand, raise the possibility of a consumer market.
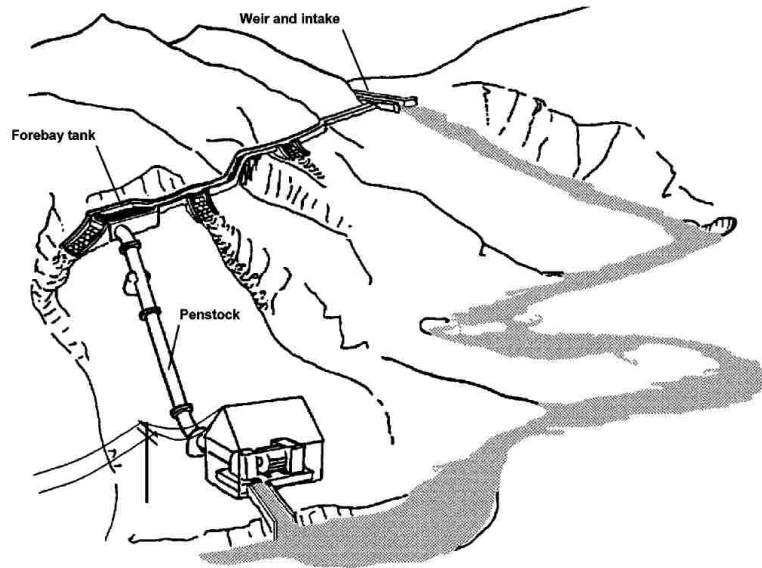
Figure 3: Layout of a small hydro instillation [6]

Computational Techniques

Computational Fluid Dynamics, or CFD, is a numerical approach to fluid dynamics utilizing finite differencing approximations. First developed by Kopal in 1947, this practice exploded in 1960's to understand the problem of a blunt body, especially when supersonic [7]. This approach has revolutionized the ability to apply basic fluid dynamics theory to real-world problems. CFD allows for immediate insight into the characteristics of a flow field when the ability to create a closed-form solution is not possible and without the need for potentially expensive testing.

The most difficult aspect of CFD lies in obtaining accurate results. This lies in three main areas: mesh generation, boundary conditions, and model usage. Several considerations need to be made about mesh generation. The structure of the mesh is very

7

important and there are a number of potential options which play into computational demands as well as accuracy. Additional considerations need to be made when dealing with highly viscous regions. Often in regions approaching a wall, the mesh is highly refined, often called inflation, to give greater detail for the second order derivative in the Navier-Stokes equations [7]. Computational models vary as well. A 2-D approach can be implemented if one of the dimensions is fairly uniform in nature. Compressibility is a concern as well as the effect of turbulence. There are a number of turbulence models that may be utilized which are specifically geared towards different scenarios [7]. Lastly, the boundary conditions play an important role. Inlets and outlets need to be considered carefully and may be specified by a variety of parameters. Walls of the domain need to be analyzed and can have a number of different types of conditions. Free surfaces, zero shear, permeable membranes and moving walls are all possible.

Finite Element Analysis, or FEA, is often used in order to determine the structural integrity in wind and hydro turbines. Patricio Gallardo wrote a thesis on the stress analysis of wind turbines in cold weather conditions. Using an approximated load, the concentration of this thesis related to the effect of cold temperature and the load on specific areas associated with the turbine such as the blade and joint in discussion [8]. Due to the unique geometries of the Archimedes screw and the hydrokinetic design, to be discussed in Chapter 2, a complete mapping of the pressure obtained from the computational fluid analyses had to be mapped onto the turbines, for multiple cases, in order to fully understand the forces acting on the turbine. Due to the small diameters of both designs, centrifugal effects were not considered as loads on the turbine as they are relatively small compared to the high force of the pressure acting directly on the blade.

Chapter 2: Design of Archimedes Screw and Hydrokinetic Turbines

Archimedes Screw
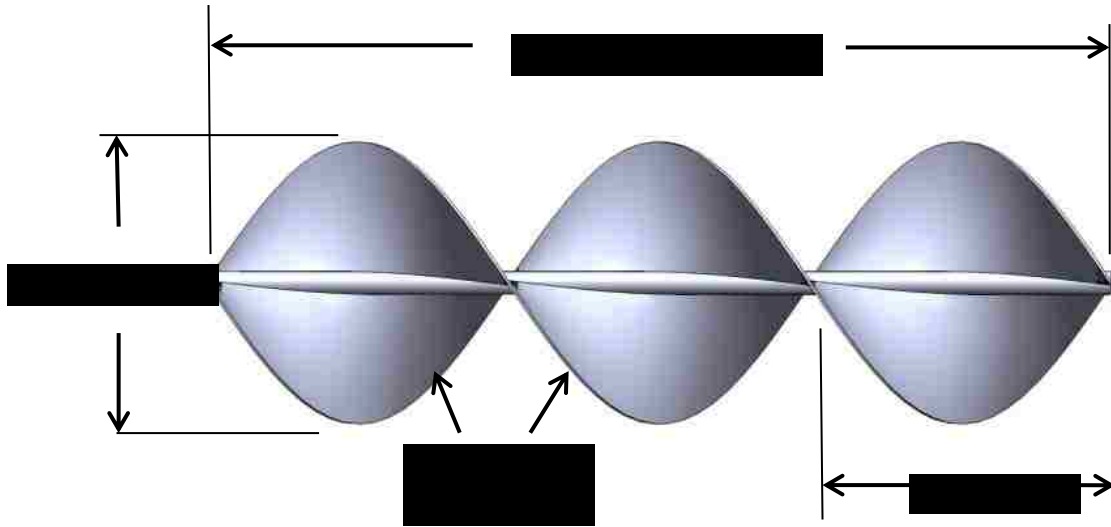
Figure 4: Diagram of the Archimedes Screw Design

The Archimedes screw design centered on optimizing the rate of pitch change throughout the length of the turbine, the pitch being longer at the entry and continually decreasing over the turbine. As seen above in Figure 4, for the sake of consistency a 6" diameter, a 19.5" runner length, and two blades were used in all simulations. In order to generate the continual pitch change, three methods were used: a constant pitch, an arctangent pitch, and power 1.5 pitch. In order to create these curves, parametric equations were created, points were defined in MatLab and imported as curves into SolidWorks. Another parameter for analysis was the number of turns of the blades; 2 ½, 3, 3 ½, and 4 turns were all considered.

The curves were parametric equations created in MatLab and exported as points to be imported into SolidWorks. The constant pitch equations were defined as:

$$X = R * \cos(t), \quad Y = R * \sin(t), \quad Z = t, \quad t = \frac{l*N*\pi}{L} \tag{1}$$

In this equation X, Y, and Z correspond to the x, y, and z coordinates where the z coordinate is along the length of the runner. R is the radius of the turbine, N is the number of turns, and L is the length of the runner. Lastly, t is a non-dimensional variable to relate the three coordinates and l is length dimension that varies from 0" to 19.5" to aid in mapping which is important in the power 1.5 and arctangent designs.

The power of 1.5 design parametric equations are as follows:

$$X = R * \cos(t), \quad Y = R * \sin(t),$$

$$Z = L * \left(1 - \left(\frac{t}{N*\pi}\right)^m\right), \quad t = \frac{l*N*\pi}{L} \tag{2}$$

Here the z-coordinate becomes much more complicated, and m corresponds to the power which in this case is 1.5.

Lastly, the equations for the arctangent design are:

$$X = R * \cos(t), \quad Y = R * \sin(t),$$

$$Z = L * \left(1 - \frac{\arctan\left(\frac{t}{N*\pi}\right)}{\arctan(1)}\right), \quad t = l * \frac{N*\pi}{L} \tag{3}$$

Depicted below in Figure 5 is a comparison of the three designs. Notice that the power 1.5 pitch offers the most rapid change at the exit of the turbine.
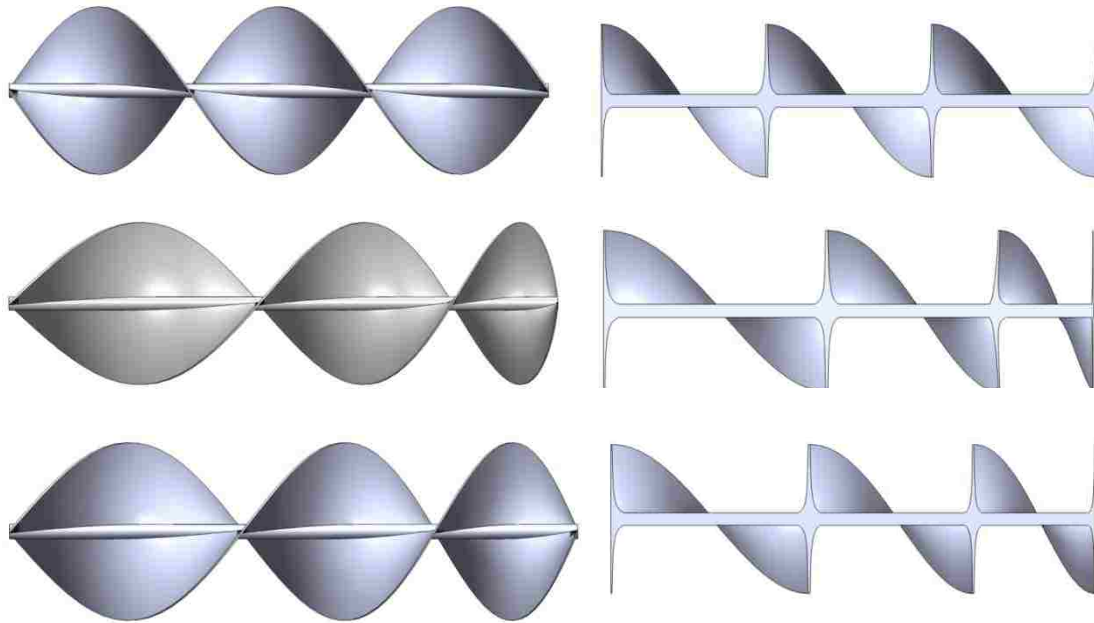
Figure 5: Comparison of the Three Designs Top to Bottom: Constant Pitch, Power 1.5, and Arctangent

In practice, the formulation of the curves was a bit more complicated. In order to fully-define the blade shape in the 3-D model, four curves were generated. Two curves for the outer edge, each with an offset in the x and y coordinates either positive or negative. Additionally two curves at the base of the shaft with the same offsets. This does mean that there is a slight change in the actual thickness of the blade from the inlet to the outlet because the normal direction changes and thus the minimum length between the front and trailing edge of the blade changes. Lastly, manipulations were made in order to keep the blade as uniform in cross section as possible. As can be seen in Figure 5 above, the blade in the arctangent design begins to warp near the exit of the turbine. This, however, was assumed to contribute a small error to the overall system analysis.

11

The purpose of the computational fluid study was to optimize the turbine over a range of rotational speeds and flow rates. This investigation was primarily conducted by Chris Schleicher and published in his thesis [9]. From this data, cases where high torque was exerted onto the runner blade were examined for a structural investigation. Several techniques were utilized for improving the structural integrity such as increasing the thickness of the blade, the shaft diameter, and adding fillets between the two surfaces where allowable as will be discussed in Chapter 4. There were limitations to the ability to add fillets between the two surfaces. SolidWorks has some difficulty generating these features between curved surfaces.

Hydrokinetic Design

While the Archimedes screw design utilizes a pressure gradient in order to generate energy, a purely kinetic design has many applications as well. Similar to how a wind turbine generates power, the concept here is to have this turbine in a free-stream river and allow the flow of the water to turn the turbine. For this concept, inspiration was taken from wind power and the aerospace industry. As a base case, a series-4 NACA 8406 airfoil was selected. A hub was constructed with a symmetric airfoil geometry being swept in a 360 degree arc with the back of the hub leveling out to a shaft diameter of 0.5". This shaft diameter was subject to change as will be discussed in Chapter 4. Then two blades were created by sweeping the NACA 8406 airfoil through a 140 degree arc at an approximate span angle of 70 degrees and extruded to base hub as seen in Figure 6,

Figure 7, and Figure 8 below. The diameter of the turbine is 21", significantly larger than the Archimedes screw design.
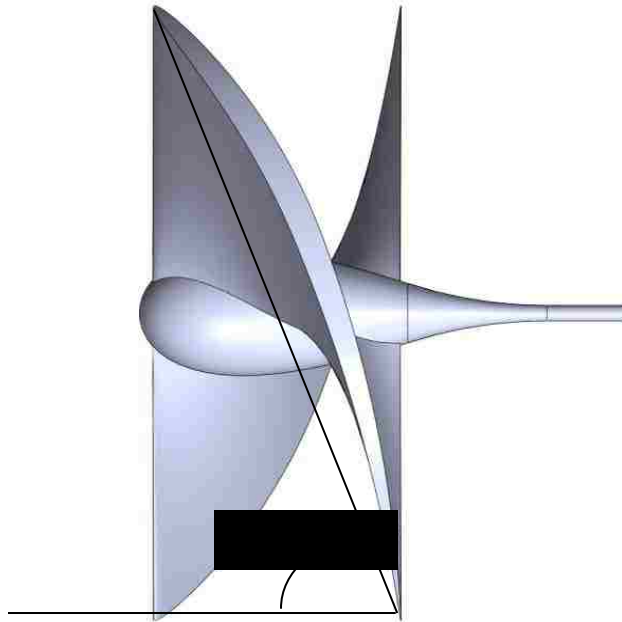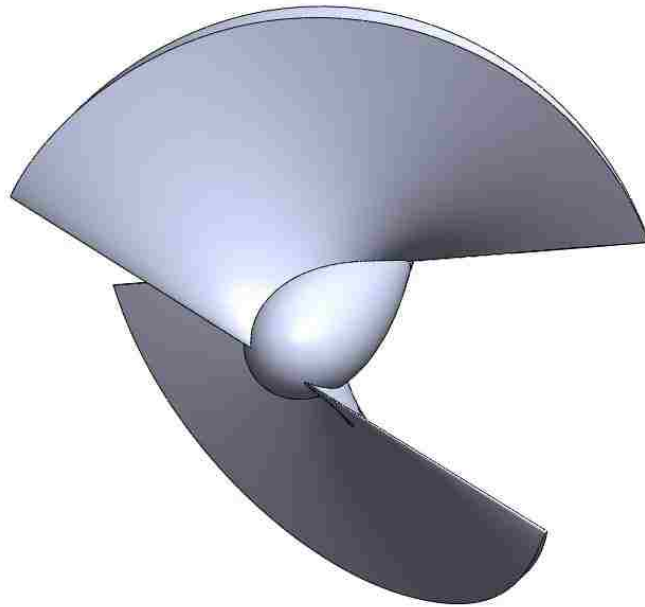

Figure 6: Top View of Hydrokinetic Design

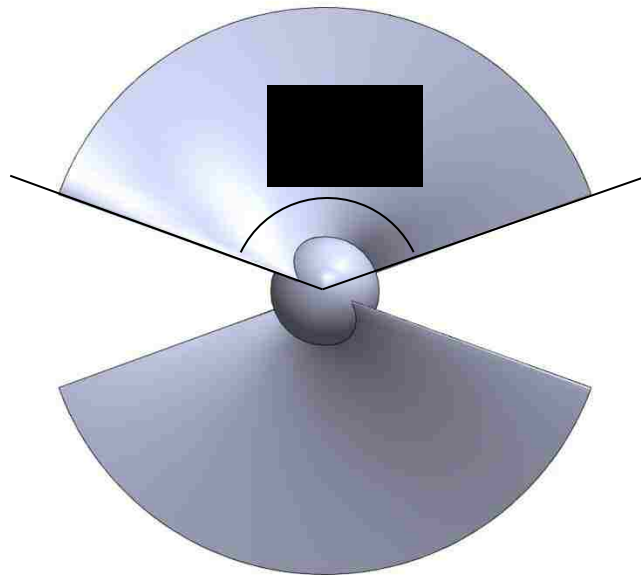Figure 7: Isometric View of Hydrokinetic Design

Figure 8: Front View of the Hydrokinetic Design

14

Chapter 3: Computational Fluid Dynamics Method and Results

Simulation Method

Prior to the onset of structural analysis a complete fluid analysis was completed primarily by Chris Schleicher and Jake Riglin for both designs aiming at finding the power and efficiencies of each design over a range of rotation rates and flow rates. Additional analysis was completed on the Archimedes screw design attempting to optimize the blade geometry for different flow rates. After this initial parameter analysis, a cavitation study was completed by Jake Riglin and published in his thesis [10], and a structural study the findings of which follow in Chapter 4.

The fluid analyses of the two designs are separated greatly by the types of systems in which they are implemented. The purpose of the Archimedes screw design is to extract energy from the pressure differential available in the form of fluid head. Conversely, the hydrokinetic design aims at converting the kinetic energy of the river water into the rotation of the turbine. The key difference being the conversion of the available head and the conversion of the kinetic energy of the water. This difference leads to some slight variations in the analyses of the two systems, but for the most part the analyses are very similar.

One of the main differences is fluid regions which need to be considered in order to analyze the system properly. In the case of the Archimedes screw design, the turbine is to be placed within piping. Although a small gap would exist in the real world, this gap is ignored due to the computational demand of the tight spacing. Additionally, the

outlet of the piping itself is considered, in the computational model, to be significantly downstream of the end of the turbine itself. This is in order for the fluid region to come to settle into quasi-equilibrium, thus correcting some issues with the outlet boundary conditions as will be discussed further shortly. The hydrokinetic design, on the other hand, features no piping and the turbine itself is simply placed into a free stream river. In order to approximate this environment the fluid region included a river, modeled as a 20' radius channel with the turbine 10' below the surface of the water. A 20' section of river in length was chosen with the turbine located in the center, in this axial direction. A second fluid region encompasses the area around just the turbine. This is a cylindrical region with a diameter of 42", with the inlet located approximately 5" in front of the turbine and the outlet approximately 55" from the end of the turbine. This was used for the rotating reference frame. These regions are shown below in Figure 9.
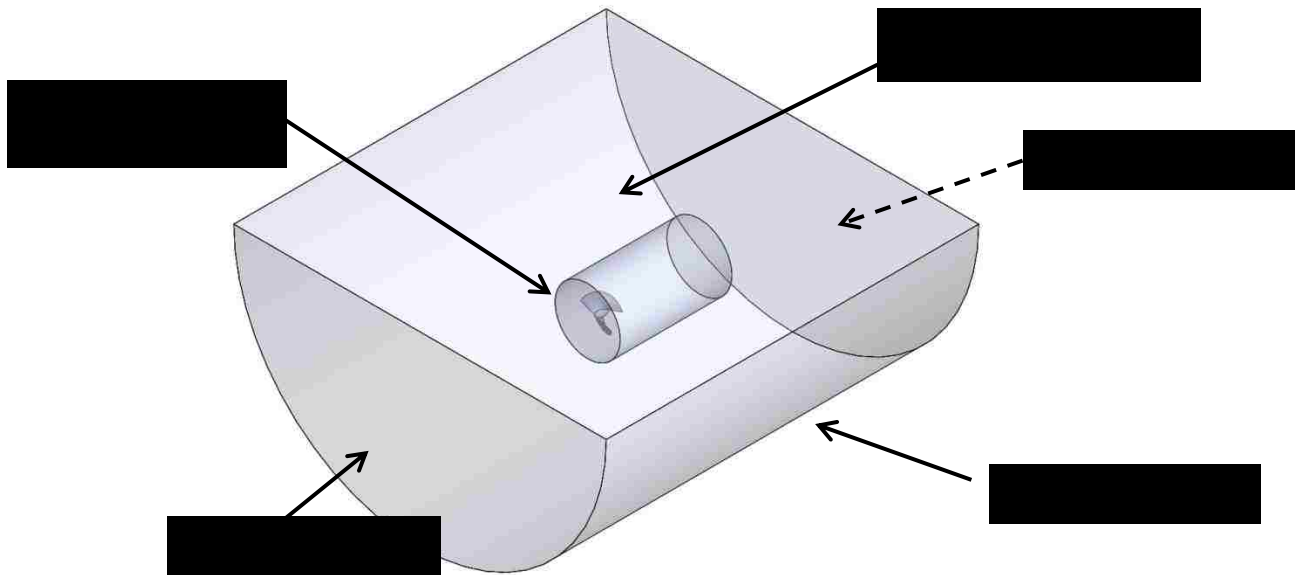

Figure 9: Hydrokinetic Fluid Regions

16

Meshing is an extremely important aspect in both designs. A simple mesh study was first conducted and the results were published in Chris Schleicher's thesis [9]. Two key features are worth mentioning. The first is that eleven layers of inflation were utilized at the surface of the turbine, the piping for the Archimedes spiral case, and the river bed for the hydrokinetic case. This mesh control was implemented due to the no slip condition that exists on these walls. This causes a relatively fast change in the velocity at these areas which requires a denser mesh to analyze properly. The second is only a factor in the hydrokinetic design. Mesh control was utilized on the interface between the outer river fluid region and the inner turbine fluid region in order to improve the quality of the mesh within the turbine fluid region and ease the transition between the two regions.

The rotation of the turbines leads to an intrinsically transient fluid problem. This rotational nature also leads to the question of how to handle the meshing of the fluid region around the turbine. There are two methods used for handling this issue. The first is to move the walls of the turbine every successive time step. This requires re-meshing the fluid region every time the domain of the turbine moves. The second method is to keep the turbine itself stationary and allow the fluid to move around the turbine region, by rotating the frame of reference. The relative calculation of the flow parameters may then be calculated with respect to this reference frame. This second method is computationally less challenging, it simply requires a few manipulations of the general fluid equations to account for the Coriolis and centripetal accelerations [11]. In the Archimedes screw design, the entire flow field is subject to this rotating reference frame, while in the hydrokinetic design only the smaller flow region located close to the turbine

was considered to be subject to this rotating reference frame. The new equations of conservation of mass and conservation of momentum are thus:

$$\frac{\partial \rho}{\partial t} + \nabla \cdot \rho \vec{v_r} = 0 \tag{4}$$

$$\frac{\partial}{\partial t}(\rho \vec{v_r}) + \nabla \cdot (\rho \vec{v_r} \vec{v_r}) + \rho(2\vec{\omega} \times \vec{v_r} + \vec{\omega} \times \vec{\omega} \times \vec{r})$$

$$= -\nabla p + \nabla * \bar{\bar{\tau_r}} + \vec{F} \tag{5}$$

In these equations ρ is the density of the fluid, t is the time, ∇ is the differential vector operator, $\vec{v_r}$ is the relative velocity vector of the fluid, $\vec{\omega}$ is the angular velocity vector, $\vec{r}$ is the radial distance to the line of rotation of the rotating reference frame, p is the pressure of the fluid, $\bar{\bar{\tau_r}}$ is the shear stress tensor, and finally $\vec{F}$ is the externally applied force.

Turbulence is another consideration that needs to be addressed. The effect of turbulence cannot be ignored in this fluid analysis, so a suitable turbulence model must be chosen. In this study, the renormalized group k-epsilon model was utilized [12]. The transport equations for this method are as follows:

$$\frac{\partial}{\partial t}(\rho k) + \frac{\partial}{\partial x_i}(\rho k u_i) = \frac{\partial}{\partial x_j}\left[\left(\mu + \frac{\mu_t}{\sigma_k}\right)\left(\frac{\partial k}{\partial x_j}\right)\right] + P_k - \rho \varepsilon \tag{6}$$

$$\frac{\partial}{\partial t}(\rho \varepsilon) + \frac{\partial}{\partial x_i}(\rho \varepsilon u_i) = \frac{\partial}{\partial x_j}\left[\left(\mu + \frac{\mu_t}{\sigma_\varepsilon}\right)\left(\frac{\partial k}{\partial x_j}\right)\right] + C_{1\varepsilon}\left(\frac{\varepsilon}{k}\right)P_k - C_{2\varepsilon}^* \rho\left(\frac{\varepsilon^2}{k}\right) \tag{7}$$

$$C_{2\varepsilon}^* = C_{2\varepsilon} + \frac{C_\mu \eta^3 \left(1 - \frac{\eta}{\eta_0}\right)}{1 + \beta \eta^3} \tag{8}$$

$$\eta = S\frac{k}{\varepsilon} \tag{9}$$

$$S = \left(2S_{ij}S_{ij}\right)^{\frac{1}{2}} \tag{10}$$

$$\mu_t = \rho C_\mu \left(\frac{k^2}{\varepsilon} \right) \tag{11}$$

In these equations t is time, ρ is the density of the fluid, ε is the turbulent energy dissipation, u is the velocity vector, x is the position vector, μ is the local dynamic viscosity, μ_t is the turbulent viscosity, k is the turbulent kinetic energy, P is the pressure, $C_{1\varepsilon}$, $C_{2\varepsilon}$, C_μ, σ_ε, and σ_k are constants, $C_{2\varepsilon}^*$ and η are parametric constants, S is the modulus of the mean rate-of-strain tensor, S_{ij} is the rate of strain tensor, and the subscripts i, j, and k are vector integers.

Boundary conditions play an extremely important role in the fluid simulation process. In both the case of both designs, the boundary condition at the inlet was considered to be a fully developed flow. The velocity equations were assumed to be the following standard relationships:

$$\frac{u}{U} = \left(1 - \frac{r}{R} \right)^{\frac{1}{n}} \tag{12}$$

$$n = -1.7 + 1.8 \ln Re_u \tag{13}$$

In these equations, u is the local velocity, U is the maximum velocity, r is the local radius, R is the outer radius of the pipe or channel, n is a parametric constant, and Re_u is the Reynolds number using the maximum velocity and the hydraulic diameter as the characteristic length. In the inlet as well as the outlet, parameters defining the turbulent kinetic energy and the turbulent dissipations rate need are calculated using the inlet and outlet parameters. These parameters are the turbulent intensity, I, and the hydraulic diameter, D_H. An empirical relation was used in order to find the turbulent intensity:

$$I = \left(0.16 Re_U^{-\frac{1}{8}} \right) * 100\% \tag{14}$$

These parameters are used to calculate the turbulent kinetic energy and dissipations rates by:

$$k = \frac{3}{2}\left(u_{avg}I\right)^2 \tag{15}$$

$$\varepsilon = \frac{C_\mu^{0.75}\left(k^{1.5}\right)}{l} \tag{16}$$

In these equations, I is the turbulent intensity, k is the turbulent kinetic energy, l is the characteristic length scale or 7% of the hydraulic diameter, ε is the turbulent energy dissipation, C_μ is a constant, and u_{avg} is the averaged velocity.

On the walls of the turbines, the piping for the Archimedes screw design, and the river bed for the hydrokinetic design the no-slip condition was used. This means that the local velocity of the fluid adjacent to these walls were zero. In the hydrokinetic case, the free surface was assumed to have a shear stress of zero.

A number of methods used in the solution procedure need to be mentioned. A simple, pressure based solver was used. This is an uncoupled technique. Second order upwind discretization was used for the turbulent kinetic energy, turbulent dissipation, and the transience calculation.

Results of Archimedes Screw CFD Simulations

The primary comparison of the three different designs was one of the primary considerations of the first level of simulations. These were simulations were conducted

for a flow rate of 0.1 m³/s and a rotation rate of 750 RPM. The 1.5 power pitch design proved to have significantly better efficiency and power than either of the other two designs. Additionally, the 3 turn design had the broadest operating range compared to the 2.5, 3.5, and 4 turn designs. For these reasons, the 3 turn 1.5 power pitch design was used for all further studies.

A full investigation into the efficiency, required head, and power over rotation rates in the range of 200 RPM to 1500 RPM and 0.05 m³/s to 0.5 m³/s was then conducted, seen below in Figure 10, Figure 11, and Figure 12. As can be expected, rotation rates and flow rates have a positive correlation to the power that is produced. A somewhat more interesting finding is the consistency in the maximum efficiency of each rotation rate. Each graph levels off at just above 70% efficiency. In this context, efficiency is the power extracted by the turbine divided by the available power from the available head. This is shown below in full below where $P_{turbine}$ is the power produced by the turbine, ρ is the density of water, g is the gravitational constant, ΔH is the head, and Q is the volumetric flow rate.

$$Efficiency\ \% = \frac{P_{turbine}}{\rho g \Delta H Q} * 100\% \qquad (17)$$
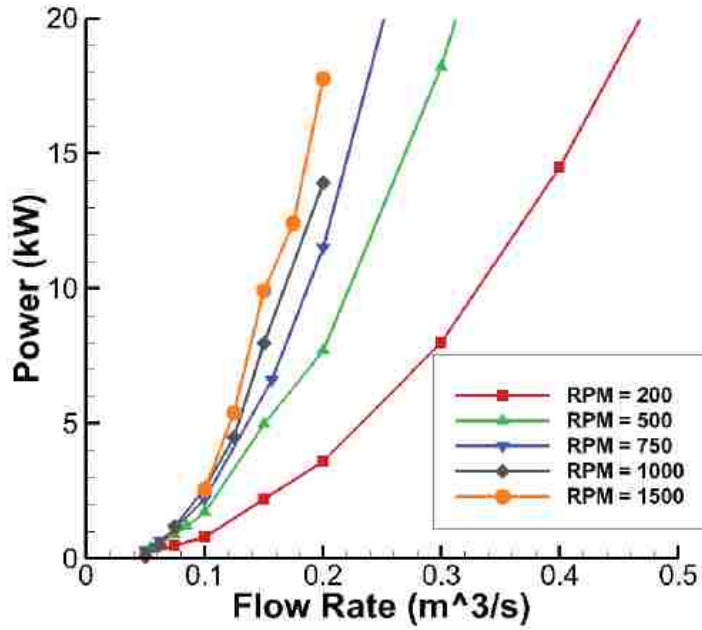
Figure 10: Power as a Function of Flow Rate and Rotation Rate for the 1.5 Power Pitch
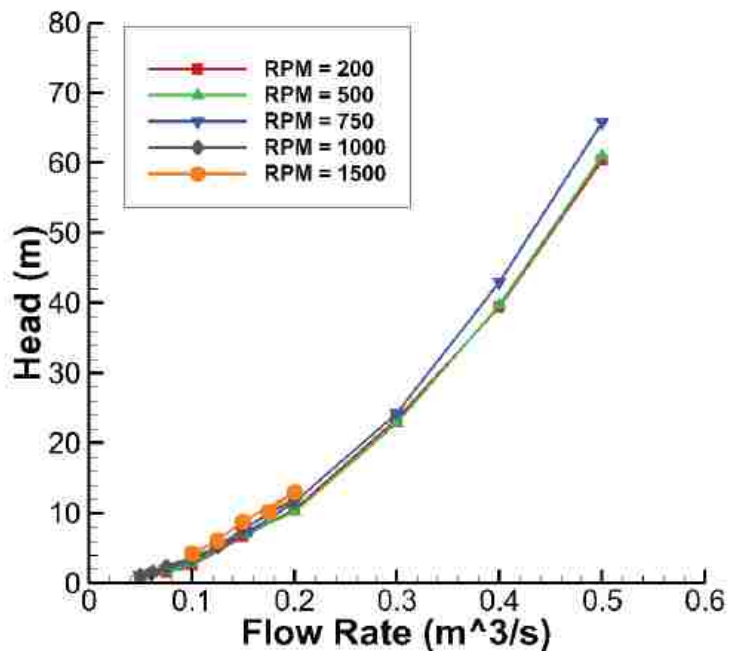
Design [9]

Figure 11: Required Head as a Function of Flow Rate and Rotation Rate for the 1.5
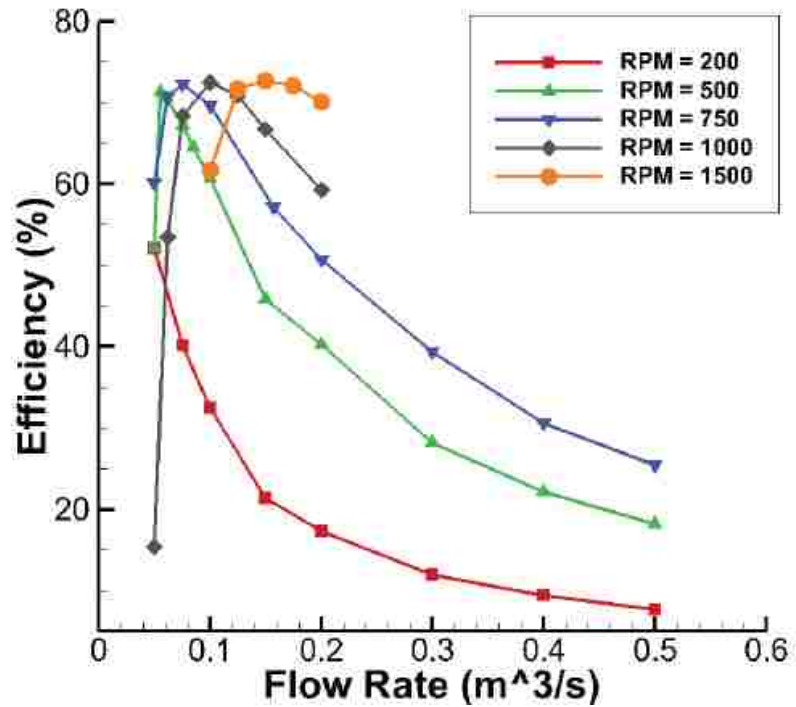
Power Pitch Design [9]

Figure 12: Efficiency as a Function of Flow Rate and Rotation Rate for the 1.5 Power

Pitch Design [9]

Following this optimization analysis 0.1 m^3/s and 1000 RPM were chosen for further structural analysis. Figure 13 and Figure 14 show the wall shear stress and pressure contours acting on the turbine blade. The effect and extent of the pressure on the blade far outweigh the wall shear stress. The wall shear stress will not be used in the structural analysis.
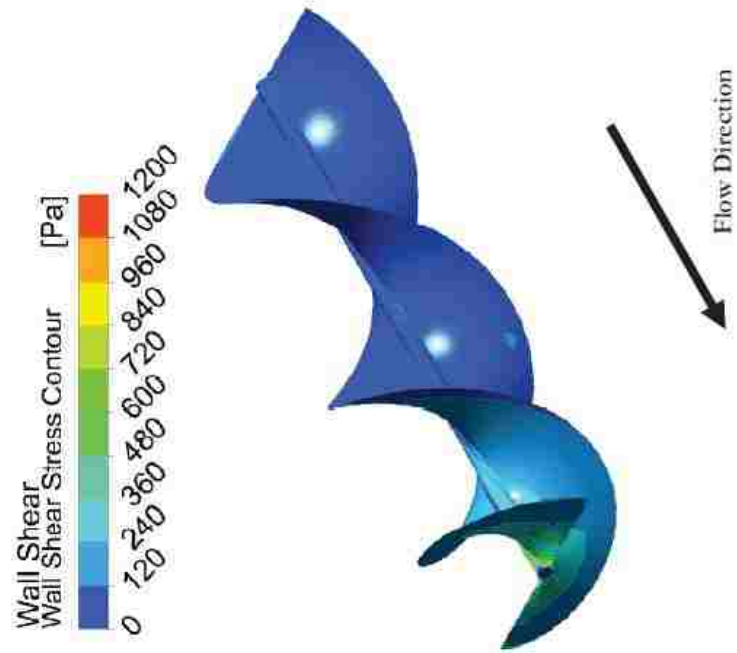
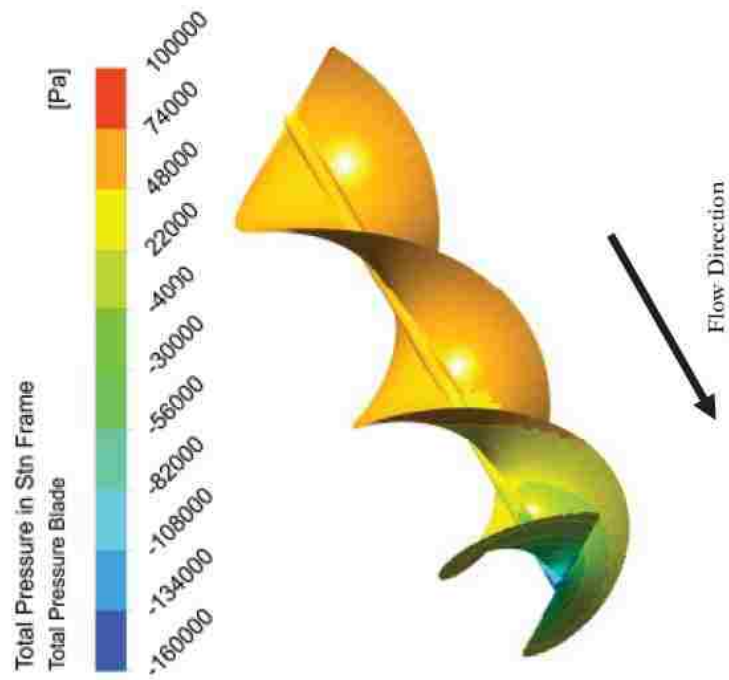Figure 13: Wall Shear Stress on Archimedes Screw Turbine

Figure 14: Pressure Acting on the Turbine Blade

Results of Hydrokinetic Simulations

For the hydrokinetic design, CFD simulations were run over a range of flow rates from 0.5 m/s to 5.0 m/s and rotation rates from 50 RPM to 225 RPM, by the group. It was found that between 3.0 and 5.0 m/s the onset of cavitation would occur and since river speeds generally do not reach this high, 4.0 m/s was selected as the highest possible case for the structural simulations with a rotation rate of 225 RPM. For these conditions the pressure contours are shown in Figure 15, Figure 16, and Figure 17. Figure 18, Figure 19, and Figure 20 show the wall shear stresses acting on the turbine blade. Again, it is clear that the main force acting on the blades is the pressure. The wall shear stress is localized mainly around the leading edge of the blades. Again, only the pressure was used in the structural simulations.
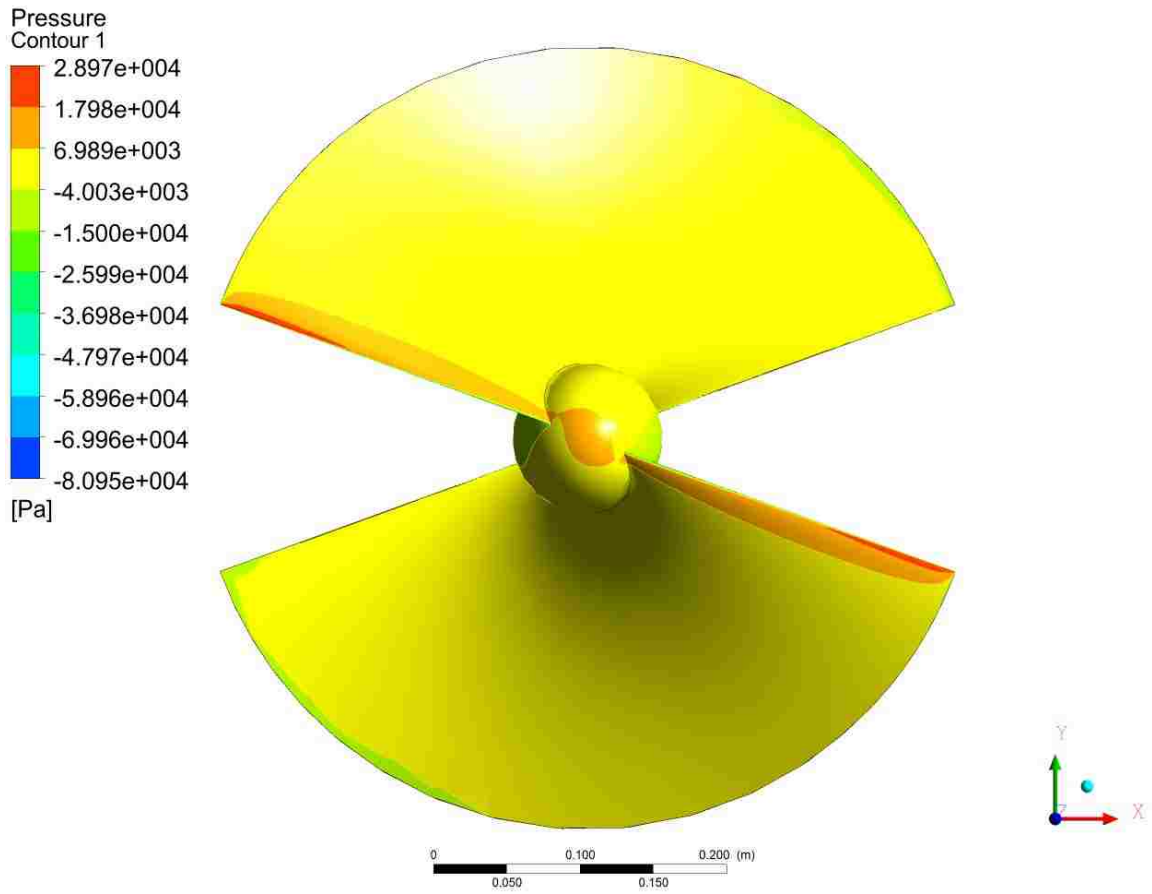
Figure 15: Pressure Contour Acting on Turbine, Front View
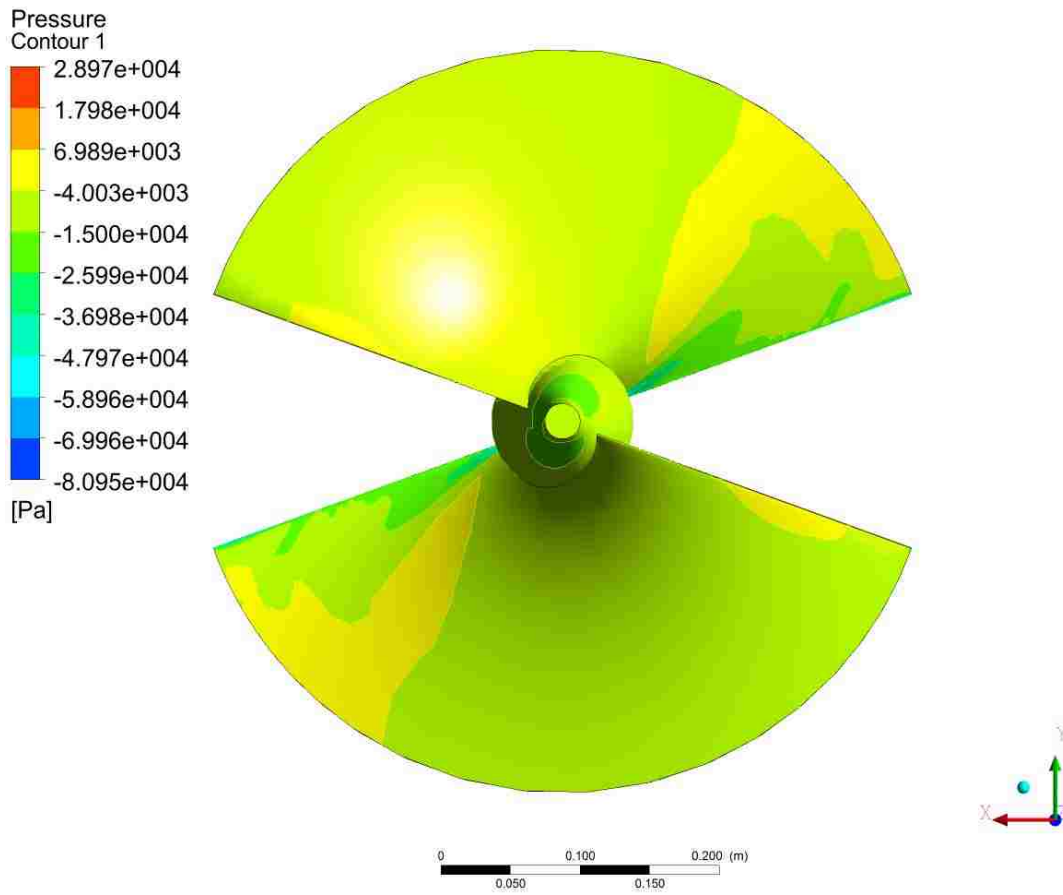
Figure 16: Pressure Contour Acting on Turbine, Back View
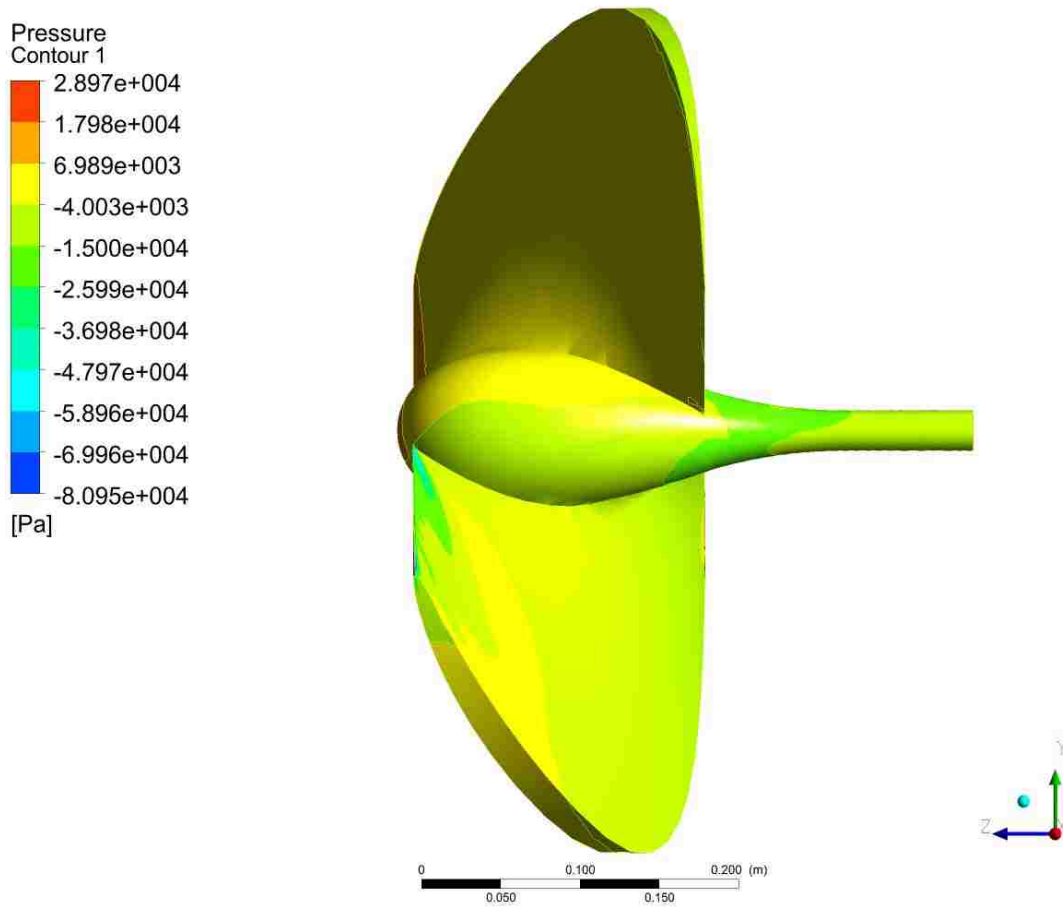
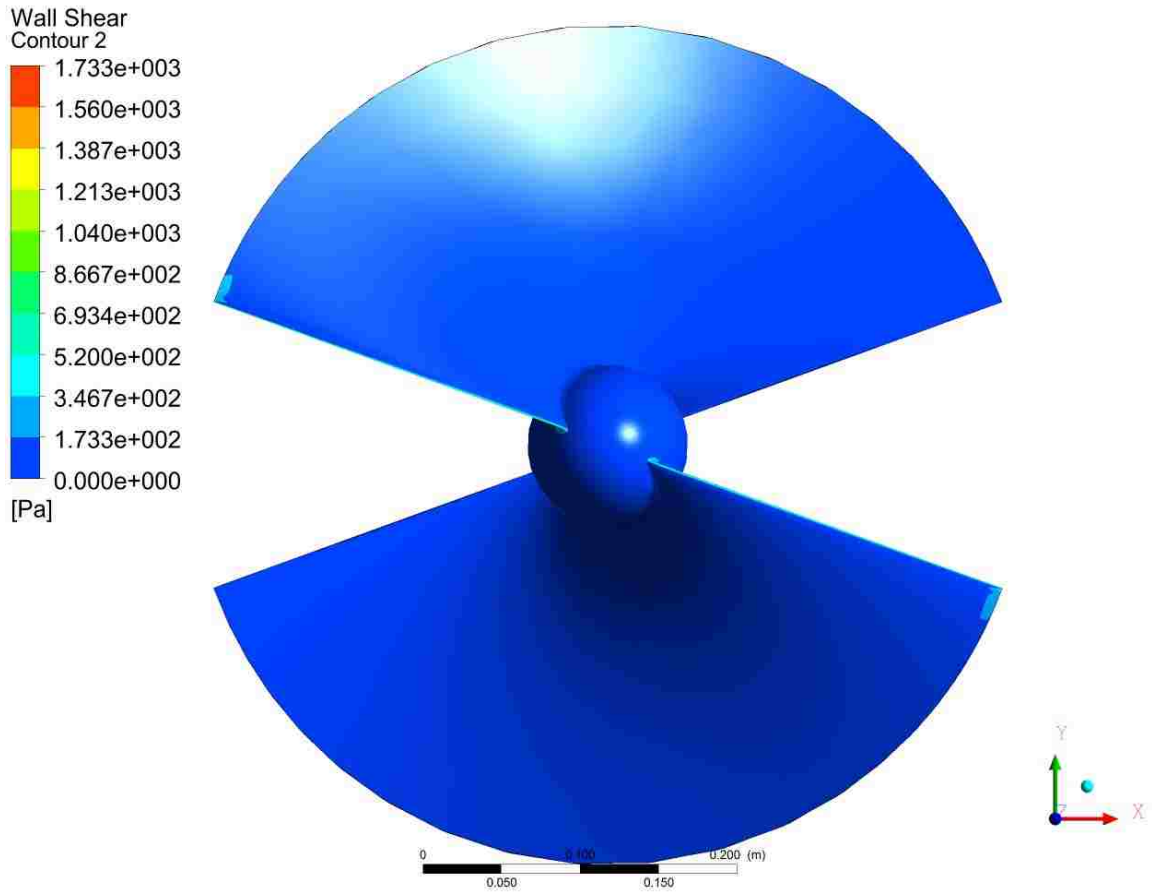Figure 17: Pressure Contour Acting on Turbine, Side View

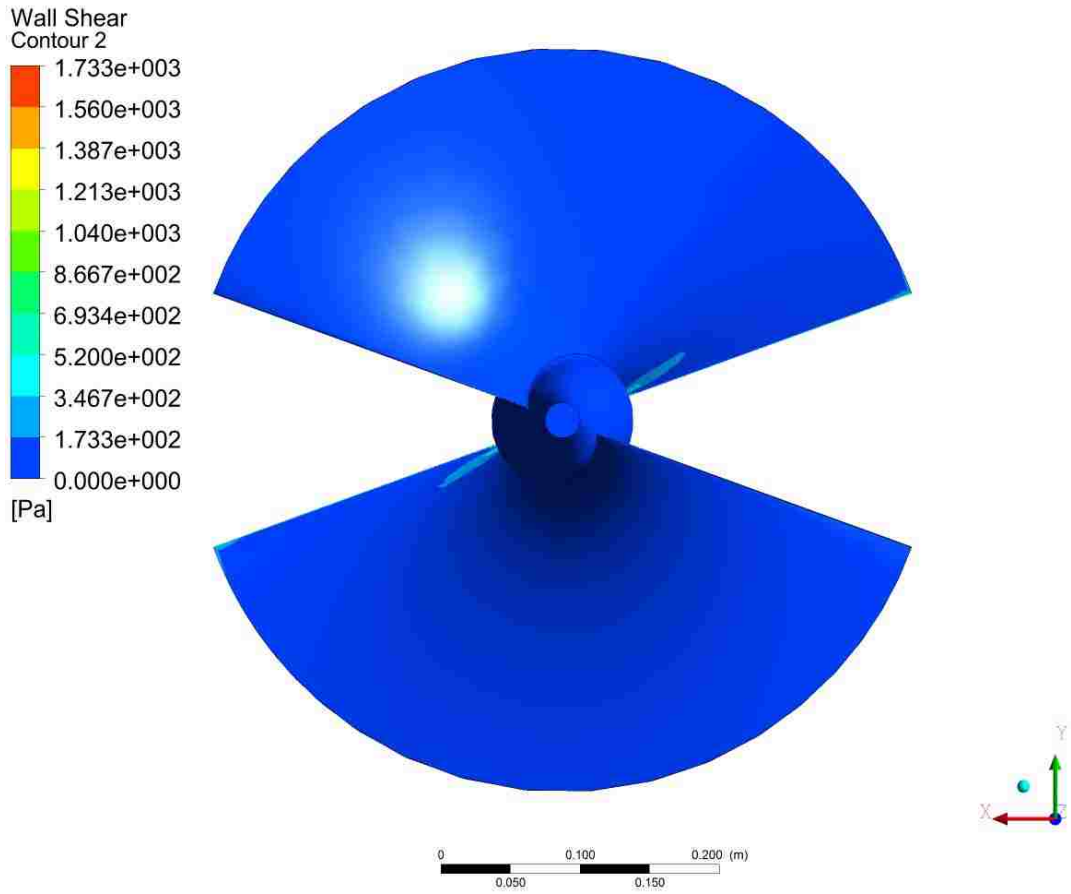Figure 18: Wall Shear Stress Acting on Turbine, Front View

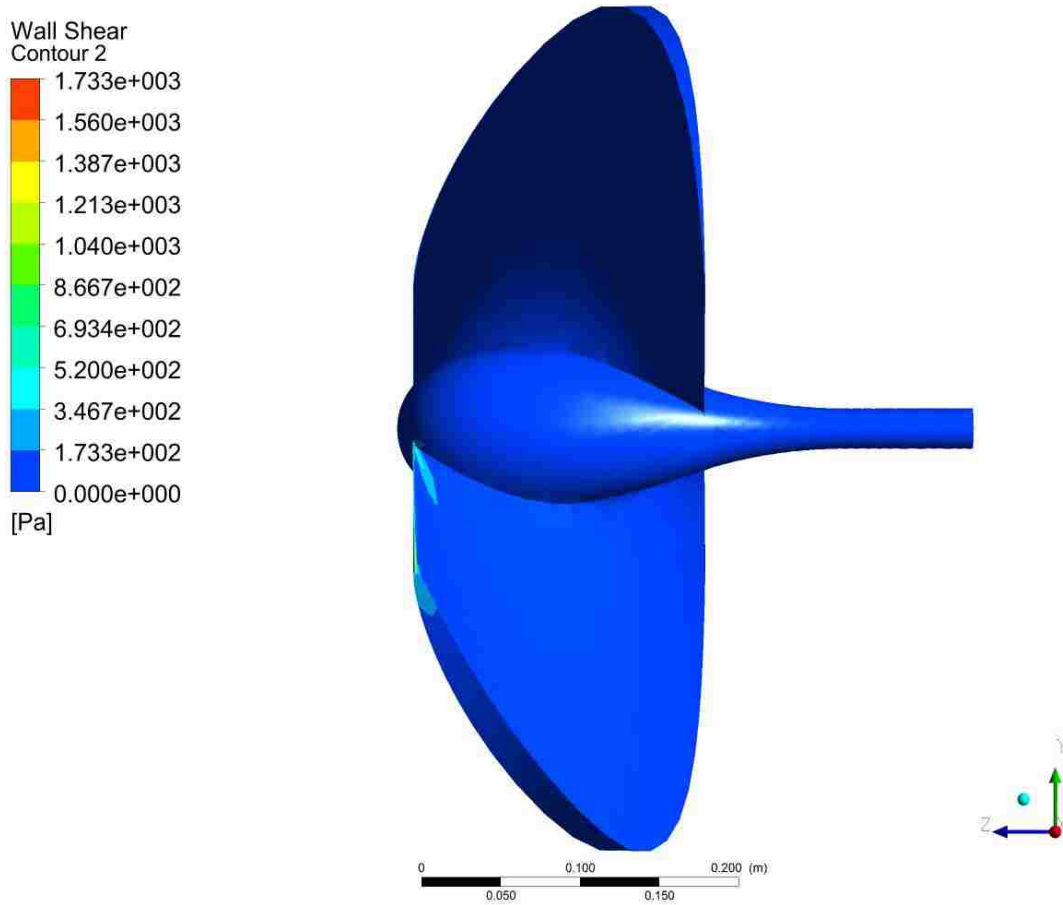Figure 19: Wall Shear Stress Acting on Turbine, Back View

Figure 20: Wall Shear Stress Acting on Turbine, Side View

Chapter 4: Finite Element Analysis

FEA Methods

The purpose of Finite Element Analysis is to discretize the overall body into a mesh of smaller elements, in this case tetrahedral elements. These small elements are then analyzed using Calculus of variation in order to minimize the error function,

approximating the stress over the entire body. The idea is to relate the force felt by each element to its displacement. In order to approximate this relationship, displacement of each element is said to be:

$$\tilde{u}(x,y) = N_j(x,y)u_j \tag{19}$$

Here, the index j can refer to any one of the element's nodes, $\tilde{u}$ is the displacement of the element, N_j is the interpolation function, and u_j is the nodal displacement. The interpolation function is assumed to be simple polynomials which are zero at all element nodes except j at which they are one. In this case a linear polynomial was used. These are then converted to a stress and strain by the relationship:

$$\tilde{\epsilon} = B_j u_j \tag{20}$$

$$\tilde{\sigma} = D\tilde{\epsilon} \tag{21}$$

$$B_j = \begin{bmatrix} N_{j,x} & 0 \\ 0 & N_{j,y} \\ N_{j,y} & N_{j,x} \end{bmatrix} \tag{23}$$

In these equations, $\tilde{\epsilon}$ refers to the approximate strain acting on the element, $\tilde{\sigma}$ is the approximate stress acting on the element, B_j is an array of the derivatives of the interpolation functions, and D is Young's Modulus. From here these stresses must be transferred correspondingly to the next element in order to find the displacement. So for this the virtual work equation can be used, resulting in the following equation:

$$f_i = \left[\int_V B_i^T D B_j dV \right] u_j \tag{24}$$

In this equation i can also be any of the nodal locations as well as j, and V refers to the volume of the element. In this way we make $\left[\int_V B_i^T DB_j dV\right]$ an approximation for the stiffness of the element.

FEA Results

In order to determine the structural integrity of the Archimedes screw design, the case which presented the highest torque was used to ensure the limitations of this design were not placed on the structural integrity. This was found to be at 0.1 m^3/s and 1000 RPM. Aluminum Alloy was ultimately selected as the material to be used as it presented a low weight and cost for what was necessary to achieve good performance. The material properties used for the analysis were yield strength of 280 MPa, 71 GPa Elastic Modulus, and Poison's Ratio of 0.33.

In these structural simulations, tetrahedral elements were used. Additionally fixed boundary conditions were placed on the face of the shaft. This means that the displacement of all the nodes on the face of the shaft were zero, both translational and rotational. Additionally von Mises yield criterion was general used to determine the structural integrity. The equation for this is shown below:

$$\sigma_v^2 = \frac{1}{2}[(\sigma_{11} - \sigma_{22})^2 + (\sigma_{22} - \sigma_{33})^2$$

$$+(\sigma_{11} - \sigma_{33})^2 + 6(\sigma_{23}^2 + \sigma_{31}^2 + \sigma_{12}^2)] \quad (25)$$

In this equation σ_v refers to the von Mises stress, σ_{11}, σ_{22}, and σ_{33} refer to the normal stresses acting on an element, and σ_{12}, σ_{23}, and σ_{31} refer to the shear stresses acting on

an element. The material then is considered to be yielding when the von Mises stress reaches the yield strength.

The first step completed was a mesh convergence study. Initially no fillets were present connecting the blade to the shaft. Due to the sharp angle, the stresses did not converge as can be seen in Figure 21. The number of nodes compared with the maximum von-Mises stress and maximum principal stress can be seen in Table 1. The refinement of the mesh was centered on the intersection of the blades and the hub as this was clear to be the area of highest inaccuracy.

Maximum Stress	Coarse Mesh	Refinement 1	Refinement 2	Refinement 3
Number of Nodal Points	18,485	47,361	109,723	157,933
Von-Mises (psi)	44140	1.1477 E5	1.203 E5	2.54 E5
Maximum Principle (psi)	53275	74753	1.452 E5	2.37 E5

Table 1 Mesh Convergence Table for Archimedes Screw with No Fillets
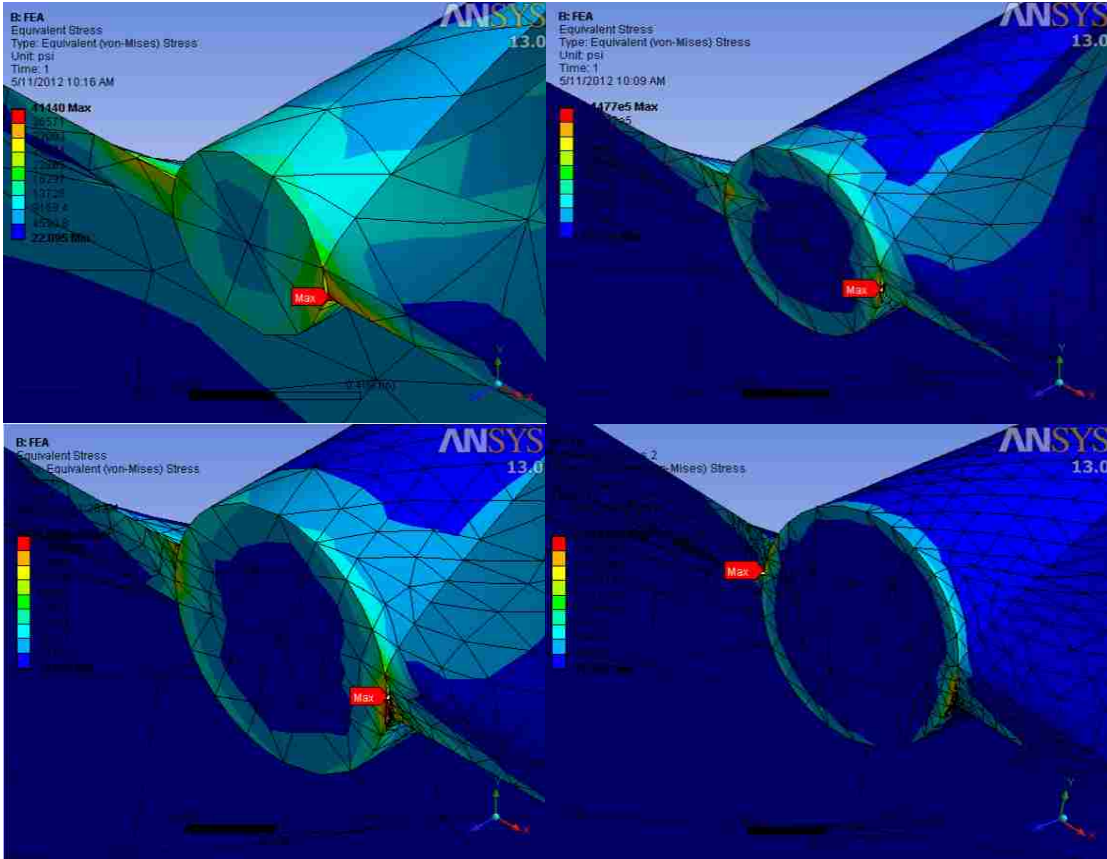
Figure 21: No Fillets Mesh Convergence

This result was not surprising due to the sharp edge between the blade and the fillet. This can often lead to an infinite stress concentration as it acts like a preexisting crack. To avoid this, fillets were added around the intersection between the blades and the shaft. This did prove difficult due to the complex geometry, but some small fillets could be added. Once added the simulations were run again, and convergence was obtained much more easily. Seen below in Figure 22, is the fully converged mesh. This mesh had approximately 212773 elements. Only triangular mesh elements were used. Much of the refinement again came around the intersection areas. Following meshing came importing the pressure distribution which can be seen in Figure 23.
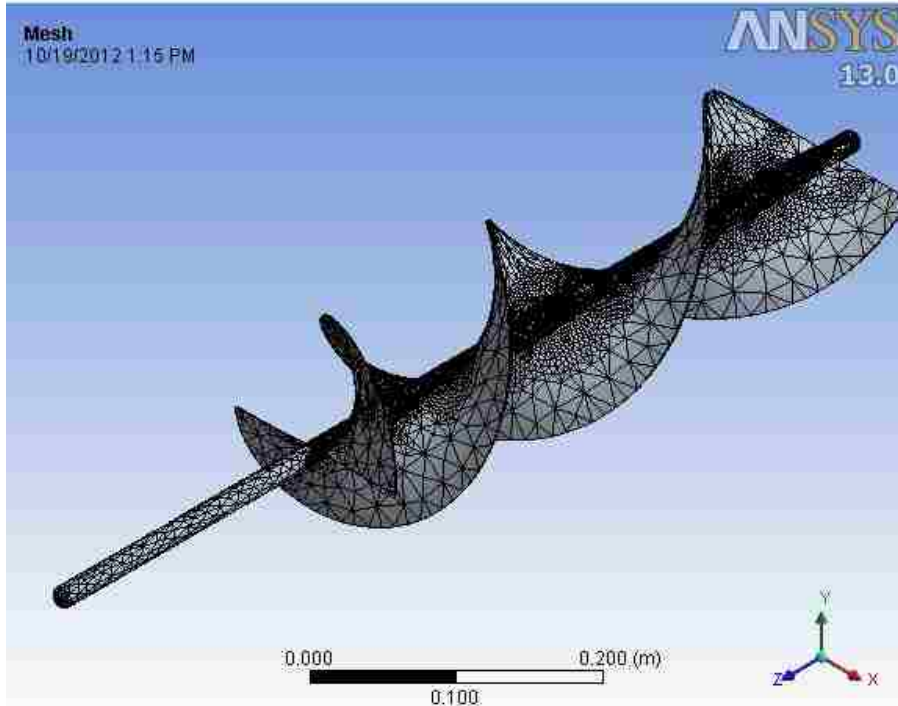
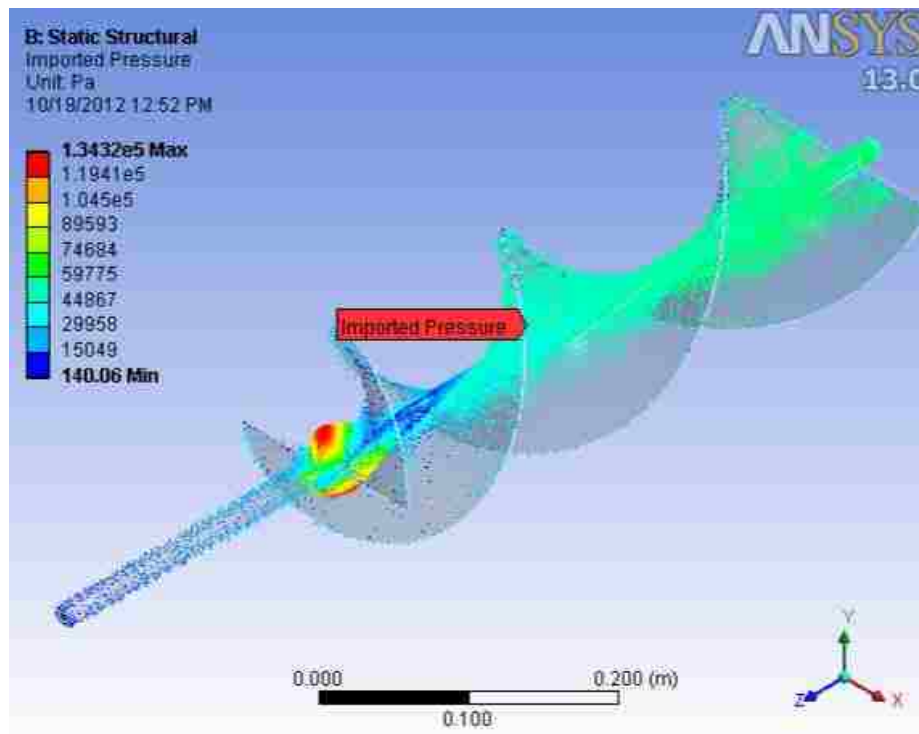Figure 22: Final Mesh for Archimedes Screw

Figure 23: Imported Pressure Distribution for Archimedes Screw

Lastly, the stresses were solved. The von-Mises Criterion was used in order to determine the stability of the design, due to the likely mode of failure being shearing of the blades from the shaft. As can be seen in Figure 24 and Figure 25, the stress reached as high as 143.67 MPa. This is just under a factor of safety of 2. A slightly higher factor of safety is preferable, but this indicates that the part is unlikely to fail as it stands and a larger fillet should take care of any concerns. The blade regions themselves appear to be safe for the most part. The stress reaches approximately 80 MPa in the blade region, which is a factor of safety of 3.5.
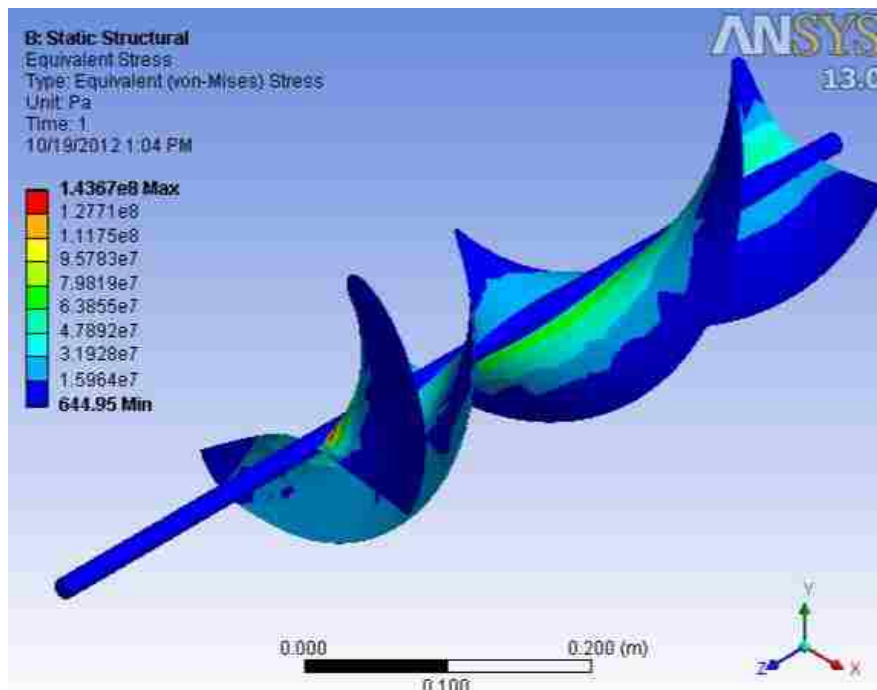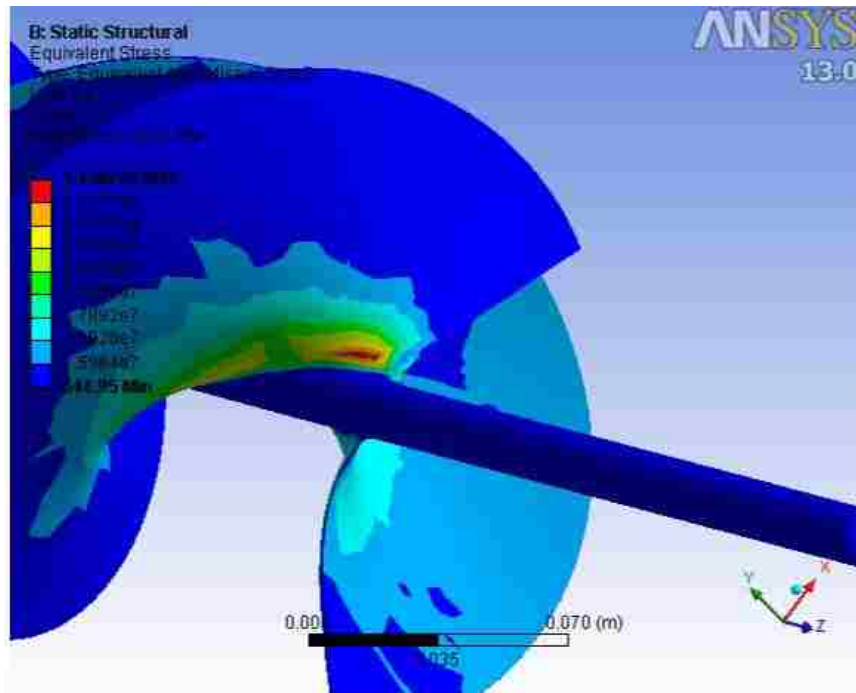

Figure 24: Isometric View of Von-Mises Stress

Figure 25: Close Up View of Von-Mises Stress

The material selected for the hydrokinetic design was also Aluminum Alloy. The first step was to analyze the first design. This featured a 0.5" shaft at the end of the hub. Simulations were conducted at a flow rate of 4 m/s and a rotation rate of 225 RPM, as these were the upper limits of the operating ranges. A fixed boundary condition was considered at the end of the shaft where the shaft would connect to the generator. Although specifically how this would be done, at this point, had not been decided, this

Again, a mesh refinement study was conducted. The fully converged mesh can be seen in Figure 26. The projected pressure distribution is shown in Figure 27. This model featured a more natural connection between the blades and the hubs so this did not pose nearly as much of a problem. A greater concern became the shaft diameter itself. The torque was fully absorbed into the shaft causing von-Mises stresses as high as 992 MPa

seen in Figure 28 and Figure 29. Due to the nature of the forces in the shaft being mostly

shearing due to torque with possibly a smaller contribution of normal stresses from

compression of shaft and bending due to an off balance in the pressure distribution, von-

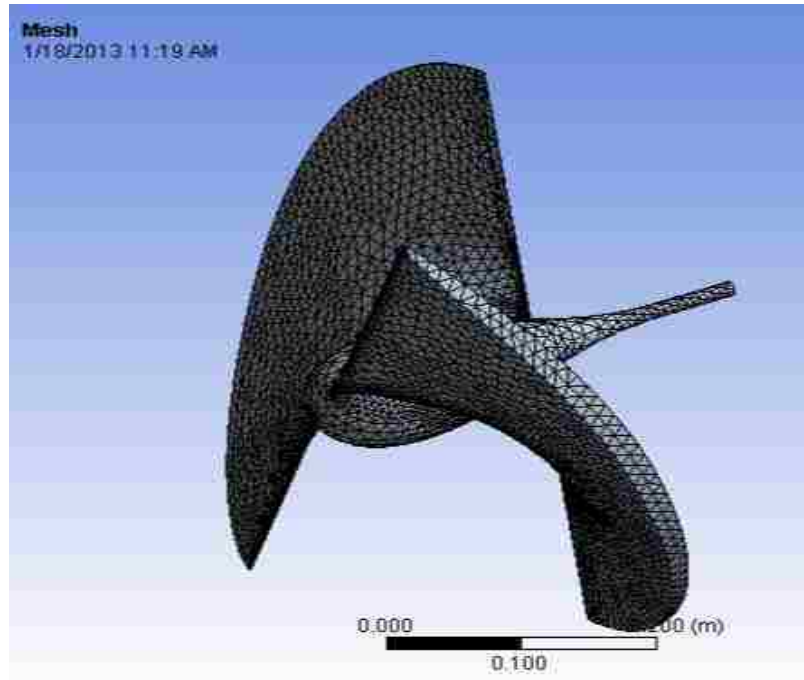Mises equivalent stress was selected as the best indicator of failure.

Figure 26 Mesh for Hydrokinetic Design with 0.5" Shaft Diameter
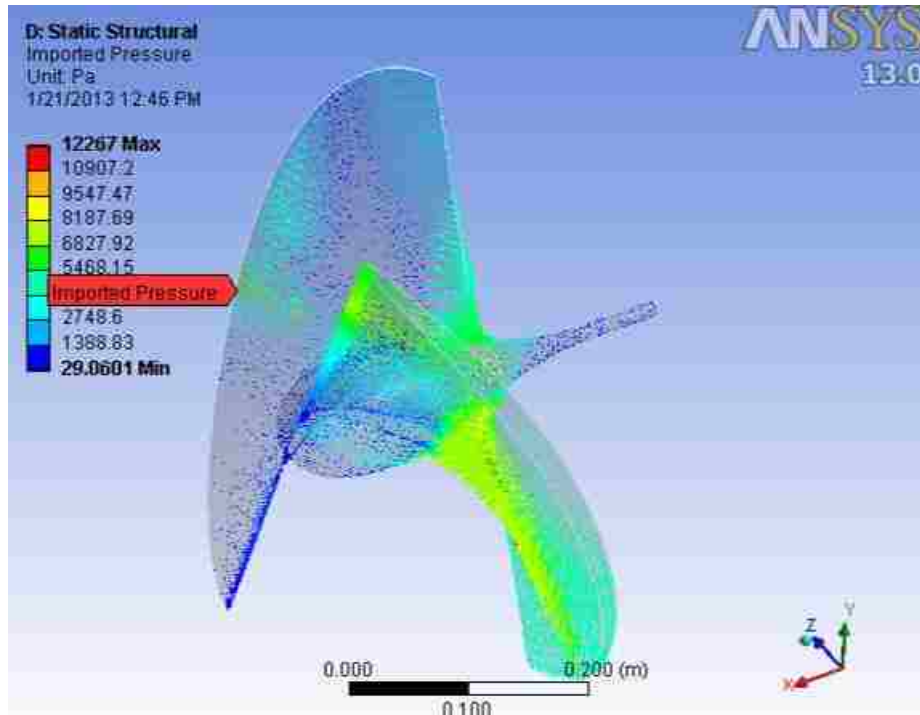
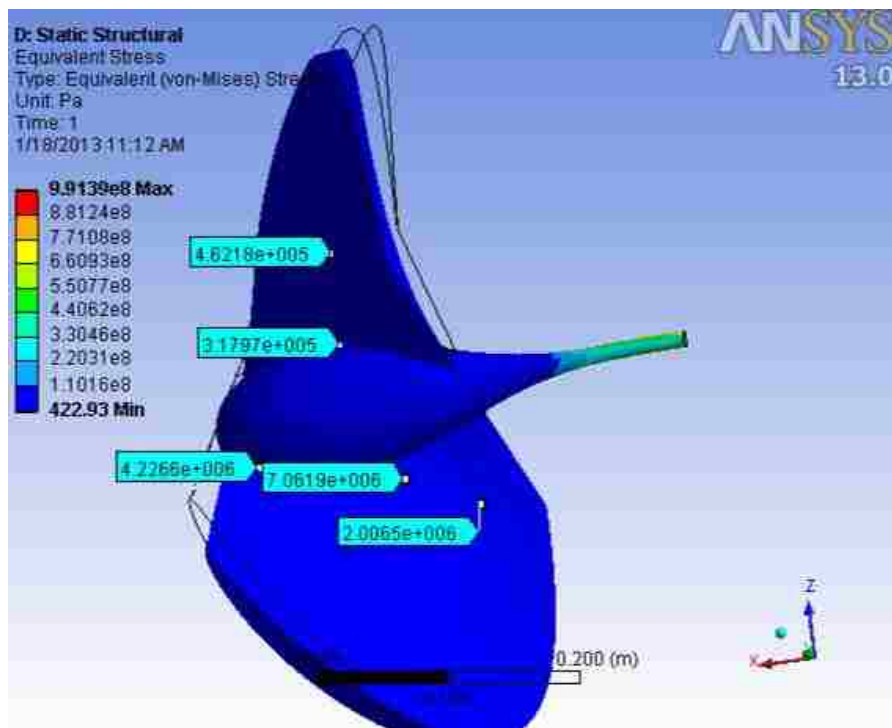Figure 27: Pressure Distribution for Hydrokinetic Design

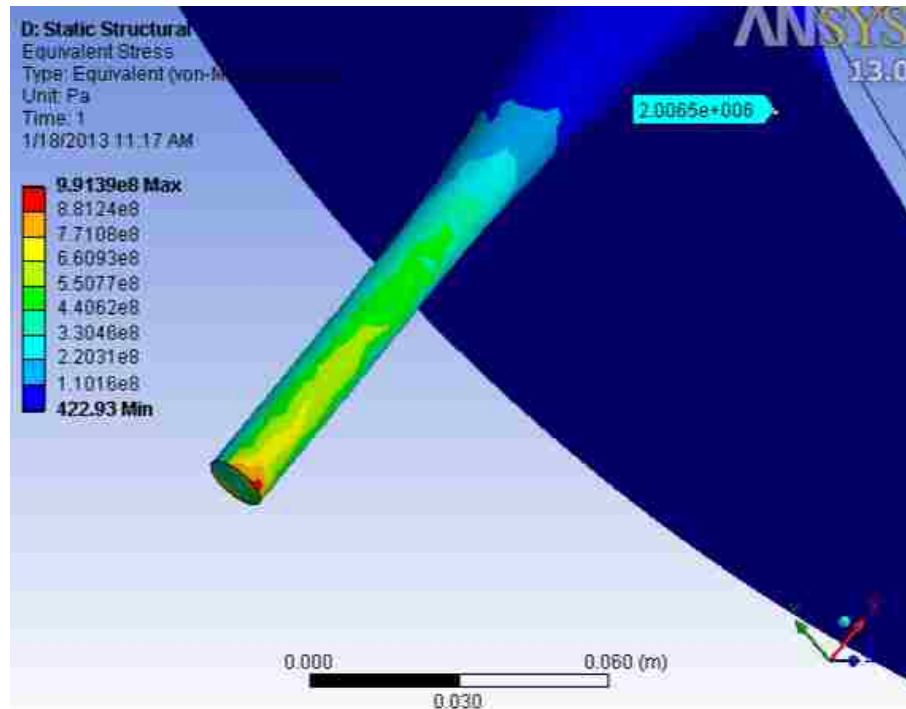Figure 28: Von-Mises Stress Distribution for Original Hydrokinetic Design

Figure 29: Von-Mises Stress Distribution, Close Up View

There is generally an inverse cubic relationship between stress and shaft diameter. With this relationship in mind and the desire to have a factor of safety for the shaft of approximately 1.5 and higher everywhere else, or in other words a decrease in the stress by a factor of approximately 5, a 1.0" diameter shaft was analyzed. Figure 30 shows the fully converged mesh for this design. This mesh contains 266,278 elements. Figure 31, Figure 32, and Figure 33 show the pressure distribution acting on the turbine.

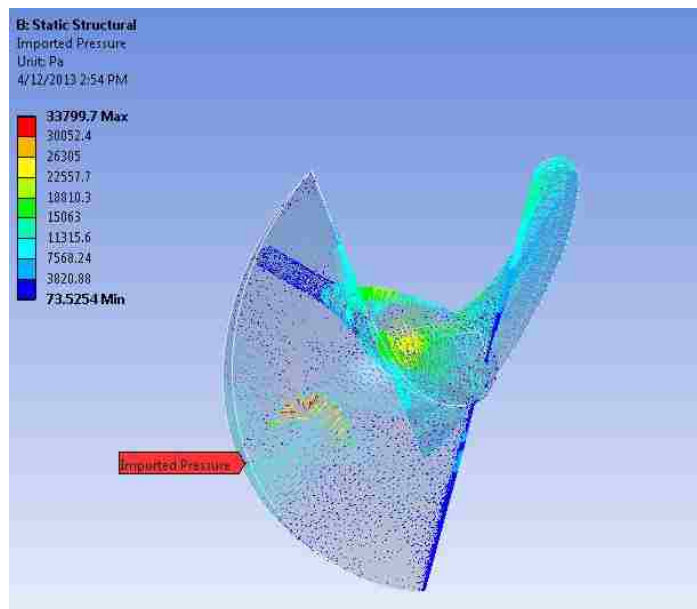Figure 30: Mesh for Revised Hydrokinetic Design

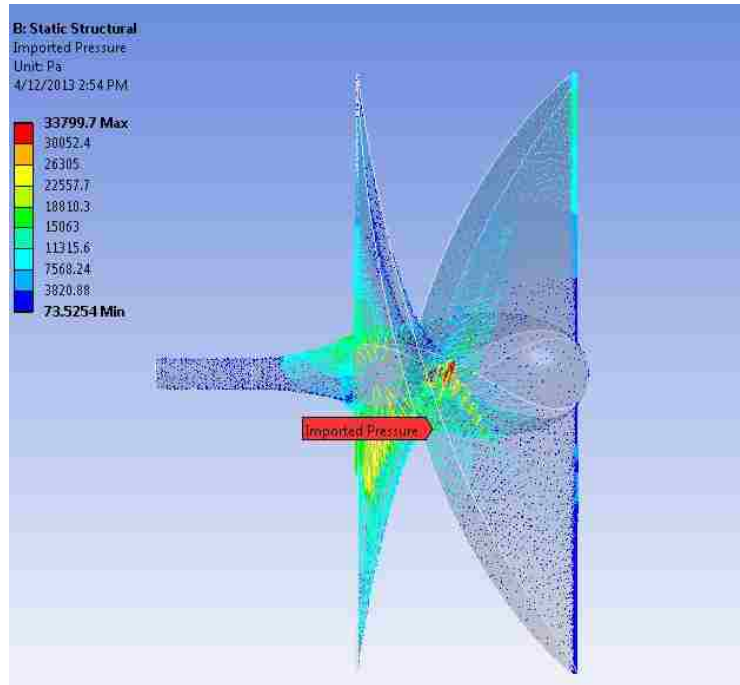Figure 31: Isometric View of Pressure Distribution
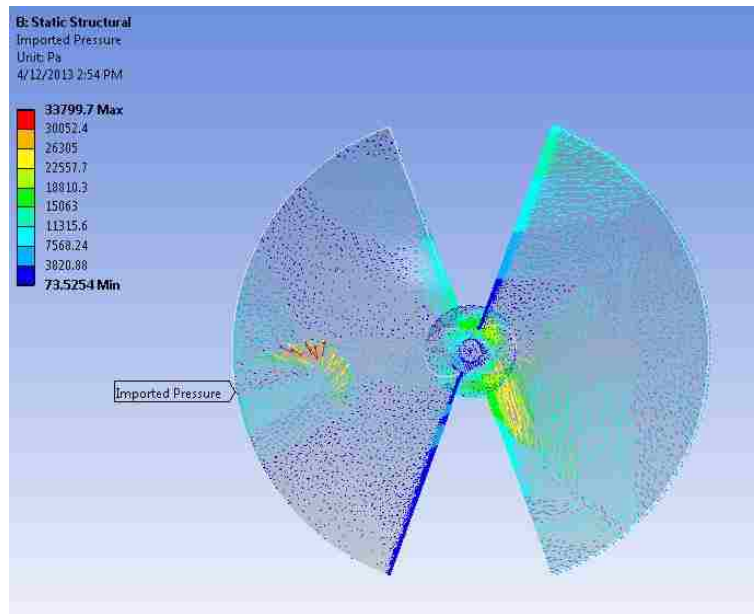
Figure 32: Side View of Pressure Distribution

Figure 33: Front View of Pressure Distribution

The results of this mechanical simulation indicate that with the factor of safety for this part is above 1.5, although a higher factor of safety is desirable, this study was done at 4 m/s which is above the operating conditions likely to be seen. Figure 34 shows the stress distribution over the entire body. As expected, the high stress is almost entirely within the shaft. CFD simulations indicate a 2% drop in the power output with this design change. While very small, increasing further this shaft diameter lowers the power output even more. A preliminary simulation with a shaft of 1.5" diameter indicated a 5% drop in the efficiency.
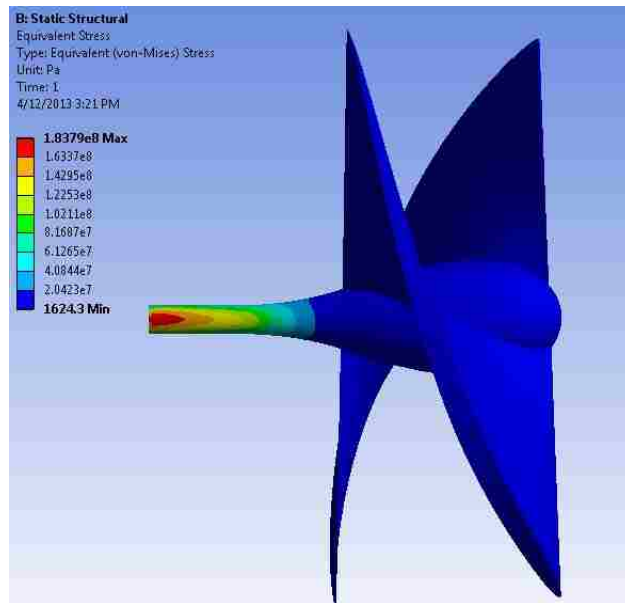

Figure 34: Side View of Von-Mises Stress

The stress distribution in the blade area and the front part of the hub is very low. Change to the blade profile and hub design may change the good results obtained from the CFD simulations. For this reason, the design was not changed to be thinner to possibly lower weight. It does yield some insight into future design considerations, as it

is now evident that the stress in these sections is not high. Figure 35 and Figure 36 show the stress in these areas. It is evident that the stress is highest at the front and tail of the blade as well as the base of the blade where intersection with the hub occurs. Special care was taken in these regions to ensure the mesh was refined.
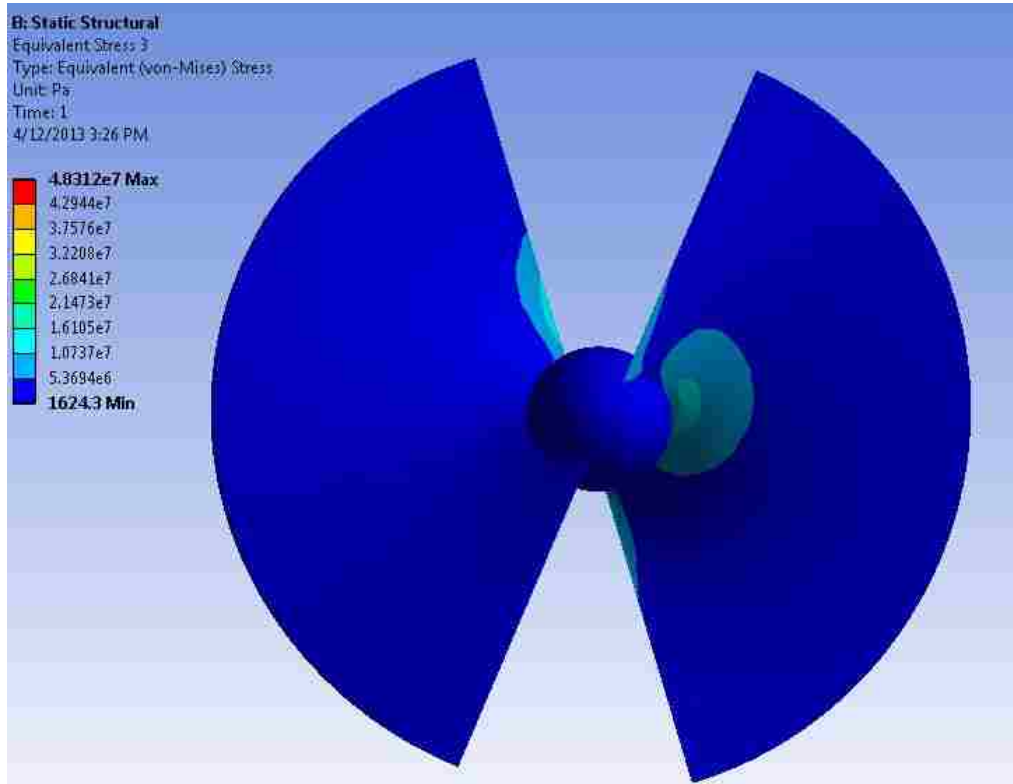

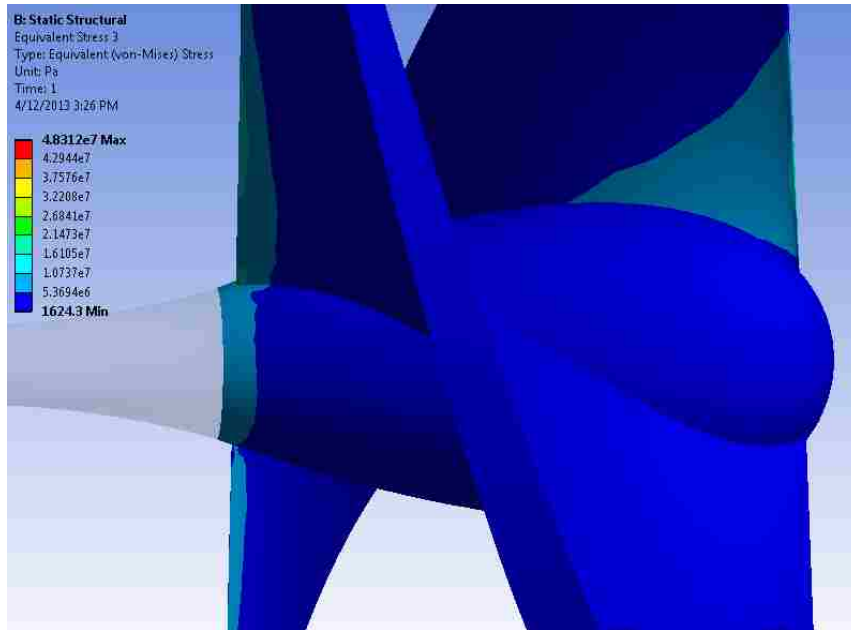Figure 35: Front View of Stress in the Blades

Figure 36: Side View of Stress in Blades

In this design the deformation of the blade is quite important. The deformation at the tip of the blade reaches 8 mm, seen in Figure 37 and Figure 38. This is a fairly considerable deflection, causing some concern about the accuracy of the CFD results. This change in the blade geometry could considerably affect the fluid flow affecting directly the power and efficiency. Additionally, this change in the fluid flow would change the stresses in the part itself as well as the dynamic stability. These issues require further investigation.
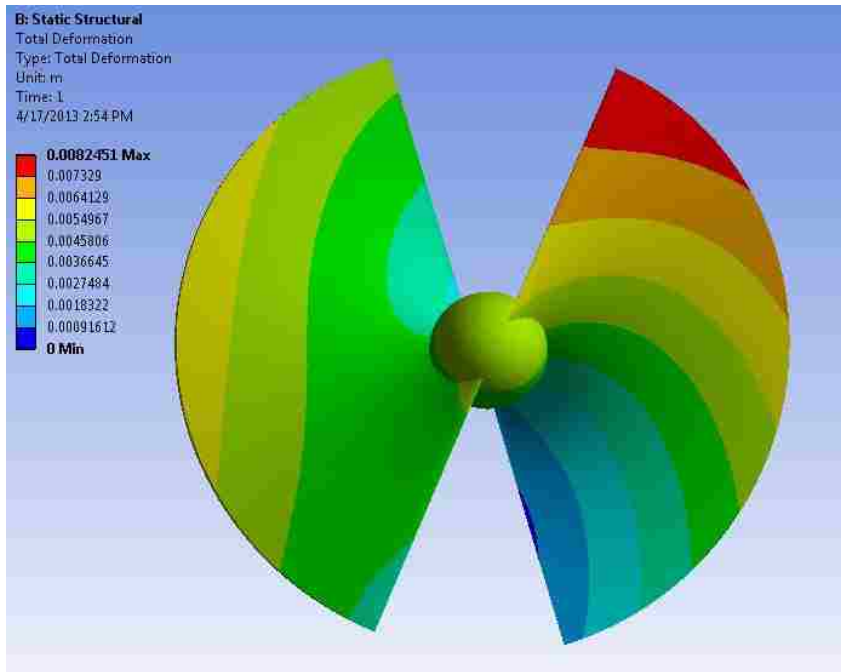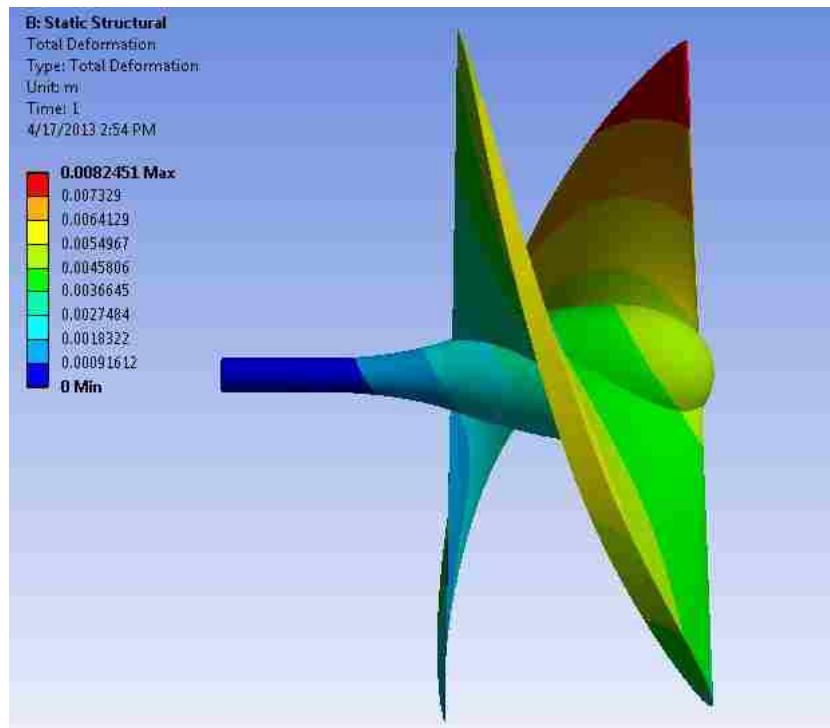
Figure 37: Total Deformation, Front View

Figure 38: Total Deformation, Side View

Chapter 5: Conclusion

Finite Element Analysis can provide an indication as to the stress felt by a part under a specific loading. For these two designs, Archimedes Screw and Hydrokinetic, first computational fluid simulations were completed for each geometry based, yielding the desired operating conditions. Further simulations were conducted to determine the forces acting on each geometry.

The investigations into both designs showed that structural stability could be achieved over a variety of operating conditions. Tetrahedral elements were used, with fixed boundary conditions on the face of the shaft. The pressure distribution was imported from CFD simulations into the FEA model. Von-Mises criterion was used as the basis of design considerations in both designs. In the hydrokinetic design this was because the highest stresses occurred on the shaft, where most of the stresses were in the form of shear stress due to the high torsion. In the Archimedes Screw design, maximum principal stresses were slightly lower than the von Mises stresses so for the sake of safety, von Misses stresses would yield a more robust design. Both designs featured stresses that cause factors of safety of at least 1.5 under the loading conditions much higher than what would generally be seen.

The limitation for improving the structural integrity of the Archimedes Screw design proved to be in modeling ability. Improvements in the structural stability of this design can be easily obtained by having a more progressive transition from blade to the shaft, however in real life this may be easier to do by simply adding a larger fillet.

The hydrokinetic design had its greatest stresses located at the end of the shaft. Due to the extremely high conditions at which this was tested, and the drop off in efficiency by further increasing the shaft diameter, changes were not made to further improve this design. The deflection found at the tip of the blade in the hydrokinetic design reached 8 mm. This requires further investigation into its effect on the efficiency and power, the resulting changes of the stress profile on the turbine, and the dynamic stability of the turbine.

BIBILIOGRAPHY

[1]   U.S. Department of the Interior, "The History of Hydropower Development in the United States," Bureau of Reclamation, 1 August 2009. [Online]. Available: http://www.usrb.gov/power/edu/history.html. [Accessed 7 April 2013].

[2]   K.E. McCarthy, "Pros and Cons of Hydropower," Connecticut Office of Legislative Research, 4 October 2010. [Online]. Available: http://cga.ct.gov/2010/rpt/20120-R-0401.htm. [Accessed 7 April 2013].

[3]   U.S. Department of Energy, "Types of Hydropower Turbines," Energy Efficiency & Renewable Energy, 11 October 2010. [Online]. Available: http://www1.eere.energy.gov/water/hydro_turbine_types.html [Accessed 7 April 2013].

[4]   Pelton Turbine HHP - V [Web Photo]. Retrieved from http://www.ecopolisla.com/en/hydro-power/products/turbines/detail pelton-turbine-hhp---v-54/

[5]   *Major hydro turbo machine types*. (n.d.). Retrieved from http://www.renewhydro.com/index3B.html

[6]   O. Paish, "Small hydro power: technology and current status," Renewable and Sustainable Energy Reviews, p. 537-556., 2008.

[7]   J.D. Anderson, J. Degroote, D. Gerard, D. Erik, R. Grundmann and J. Vierendeels, Computational Fluid Dynamics: An Introduction, 3rd ed., J. F. Wendt, Ed., Eagle River, WI: Springer, 2009.

[8]   P. A. L. Gallardo, "Static and Fatigue Analysis of Wind Turbine Blades Subject to Cold Weather Conditions Using Finite Element Analysis," University of Victoria, 2001.

[9]   W.C. Schleicher, "Numerical Invesitgation and Performance Characteristic Mapping of an Archimedes Screw Hydroturbine," Lehigh University, Bethlehem, 2012.

[10]   J. Riglin, "Cavitation Study for a Microhydro Turbine," Lehigh University, Bethlehem, 2012.

[11]   ANSYS, Inc., "Theory Guide," 2009.

[12]   V. Yakhot, S. A. Orszag, S. Thangam, T.B. Gatskiand C.G. Speziale, "Development of turbulence models for shear flows by a double expansion

technique," *American Institute of Physics,* vol. 4, no. 7, pp. 1510-1520, July 1992.

VITA

Zachary Kraybill was born in Lancaster, PA on May 24, 1990, to Bonnie and Steve Kraybill. He graduated from Manheim Township High School in Lancaster, PA in May 2008. Following high school he attended Lehigh University where he received a Bachelor of Science in Mechanical Engineering in December 2011. In January 2012, he began a graduate program in Mechanical Engineering at Lehigh University.